MS109

Micromedia Limited

The contents of this microfiche are copyright by the publisher of the original document. Please contact the original publisher for guidance in copyright matters.

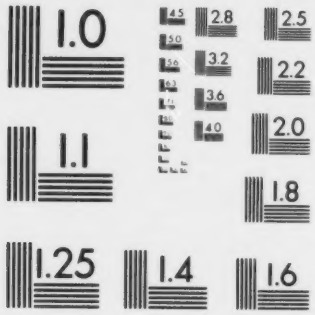

MICROCOPY RESOLUTION TEST CHART
NATIONAL BUREAU OF STANDARDS
STANDARD REFERENCE MATERIAL 1010a
(ANSI and ISO TEST CHART No. 2)

This statement was filmed with this document. If the pages of the document are less clear than this statement it is due to the poor photographic quality of the document.

NATIONAL MICROGRAPHICS ASSOCIATION

24x

PARTS OF THE ORIGINAL DOCUMENT

ARE OF POOR REPRODUCTIVE QUALITY

CERTAINES PARTIES DU DOCUMENT ORIGINAL

SONT DE PIÈTRE QUALITÉ DE REPRODUCTION

Energy, Mines and Resources Canada
Énergie, Mines et Ressources Canada

CANMET

Canada Centre for Mineral and Energy Technology
Centre canadien de la technologie des minéraux et de l'énergie

STABILITY ASSESSMENT OF S-L-102-17 SILL PILLAR OF THE NIOBEC MINE, CHICOUTIMI, QUEBEC - PART III

Y.S. YU, A.S. WONG, S. VONGPAISAL AND N.A. TOEWS
Canadian Mine Technology Laboratory

July 1987

This document is an unedited internal report prepared primarily for discussion and limited circulation. It does not represent a final expression of the opinion of the Canada Centre for Mineral and Energy Technology (CANMET)

Ce document est un rapport provisoire non-révisé et rédigé principalement pour fin de discussion et de documentation interne. Il ne représente nullement l'expression définitive de l'opinion du Centre canadien de la technologie des minéraux et de l'énergie (CANMET)

57 pp

MINING RESEARCH LABORATORIES
DIVISION REPORT MRL 87-96 (TR)

MICROMEDIA

88-02649/

STABILITY ASSESSMENT OF S-L-102-17 SILL PILLAR OF THE NIOBEC MINE, CHICOUTIMI, QUEBEC - PART III

by

Y.S. Yu*, A.S. Wong**, S. Vongpaisal*, and N.A. Toews*

ABSTRACT

A series of co-operative research studies on mine stability has been carried out with the participation of Niobec Mine, Chicoutimi, Quebec. Part III in part involves a stability evaluation of S-L-102-17 sill pillar and adjacent areas under measured mine stress conditions. The pillar is located in the upper level of Zone 1. Analytic studies were also carried out to evaluate the effect of partial extraction of the pillar on the overall stability of the upper 300 level. Three-dimensional finite element techniques were used in these studies.

It was established that under actual field stress conditions the effect of mining C-102-17 and C-102-19 stopes (2nd level) on ground stability conditions around C-102-23 stope would be nominal.

Based on the use of Drucker/Prager yield criterion and Hoek and Brown's empirical failure criterion, and assumptions concerning in situ rock properties, analytic studies indicated no potential failure zones. However, tensile stresses did occur in stope walls and pillars with a maximum value of 1.9 MPa. Therefore, localized tensile failure was established as a possibility if joints were unfavorably oriented with respect to tensile stresses.

The height of L-102-17 pillar will exceed 235m when sill pillar S-L-102-17 is partially extracted. Under these geometrical conditions localized tensile failure is possible with initial failure occuring at about one-eighth of the pillar height measured from the pillar toe. Such failures could jeopardize the pillar's stability and the stability of stopes in the upper 300 level. Therefore, early removal of the sill pillar is not recommended.

Key words: Niobec Mine, stability, three-dimensional stresses, factor of safety, finite element,

* Research Scientists, ** Physical Scientist, Mining Research Laboratories, CANMET, Energy, Mines and Resources Canada, Ottawa.

ÉVALUATION DE LA STABILITÉ DU PILIER DE SOLE S-L-102-17 À LA MINE NIOBEC CHICOUTIMI (QUÉBEC) - 3e PARTIE

par

Y.S. Yu*, A.S. Wong**, S. Vongpaisal* et N.A. Toews*

RÉSUMÉ

Une série d'études en commun portant sur la stabilité de mine a été réalisée, de concert avec la Mine Niobec, Chicoutimi (Québec). La troisième partie du rapport traite de l'évaluation du pilier de sole S-L-102-17 et des régions avoisinantes dans des conditions de contraintes mesurées. Le pilier se trouve au niveau supérieur de la Zone 1. On a également effectué des études analytiques en vue d'évaluer les conséquences de le récupération partielle du pilier sur la stabilité globale du niveau supérieur 300. Les études ont été réalisées au moyen d'une méthode d'éléments finis tri-dimensionnelle.

On a démontré que dans les conditions de contraintes réelles auxquelles le terrrain est soumis, les conséquences de l'exploitation des chantiers C-102-17 et C-102-19 (2e niveau) sur la stabilité des terrains aux alentours du chantier C-102-23 auraient peu d'importance.

Les études analytiques fondées sur le critère de rendement Drucker/Prager et le critère empirique de résistance à la rupture de Hoek et Brown ainsi que sur les hypothèses relatives aux propriétés en place du roc, n'ont indiqué aucune zone potentielle de rupture. Cependant, des contraintes de traction d'une valeur maximale de 1,9 MPa sont produites dans les parois des chantiers et des piliers. Par conséquent, on a établi qu'une rupture en traction localisée se produira si les joints ne sont pas orientés de façon à éviter les contraintes de traction.

La hauteur du pilier L-102-17 sera supérieure à 235 m quand le pilier de sole (S-L-102-17) sera partiellement récupéré. Une telle structure géométrique risque de donner lieu à une contrainte de tractiive localisée suivie de rupture initiale au huitième de la hauteur du pilier, mesurée de sa base. Des ruptures de cette nature pourraient compromettre la stabilité du pilier et des chantiers du niveau supérieur 300. Par conséquent, une récupération hâtive du pilier de sole n'est pas avisé.

Mots-clé: Mine Niobec, stabilité, contraintes tri-dimensionelles, facteur de sécurité, éléments finis.

* Chercheurs scientifiques, ** Chercheur en science physique, Laboratoires de recherche minière, CANMET, Énergie, Mines et Ressources Canada, Ottawa.

CONTENTS

	page
ABSTRACT	i
RÉSUMÉ	ii
1.0 INTRODUCTION	1
2.0 THE NIOBEC MINE	1
2.1 3-D Niobec Mine Model	4
2.2 Material Properties of the Mine Rocks	9
2.3 Field Stresses	10
3.0 RESULTS	10
3.1 Stress Distribution	11
3.2 Potential Failure Areas	20
3.2.1 Drucker/Prager Yield Criterion	20
3.2.2 Hoek and Brown's Empirical Failure Criterion	29
3.3 Average Pillar Stresses and Strength	31
4.0 CONCLUSIONS AND RECOMMENDATIONS	36
5.0 ACKNOWLEDGEMENTS	37
6.0 REFERENCES	37
APPENDIX A	39

FIGURES

1. A plan view of the Niobec Mine at Level 300	2
2. A longitudinal section at 150 + 50N	3
3(a). An isometric view of the 3-D Niobec Mine model	5
3(b). The finite element discretization for section x = 106.68 m	6
3(c). The finite element discretization for section x = 99.09 m	7
3(d). The finite element discretization for section x = 0.0 m	8
4. Major principal stress contour, for section x = 102.87m: (a) mining stage 1, (b) mining stage 2, and (c) mining stage 3.	12
5. Major principal stress contour, for section x = 95.25m: (a) mining stage 1, (b) mining stage 2, and (c) mining stage 3.	13
6. Major principal stress contour, for section x = 88.39m: (a) mining stage 1, (b) mining stage 2, and (c) mining stage 3.	14

page

7. Major principal stress contour, for section x = 82.29m: (a) mining stage 1, (b) mining stage 2, and (c) mining stage 3. 15
8. Minor principal stress contour, for section x = 102.87m: (a) mining stage 1, (b) mining stage 2, and (c) mining stage 3. 16
9. Minor principal stress contour, for section x = 95.25m. (a) mining stage 1, (b) mining stage 2, and (c) mining stage 3. 17
10. Minor principal stress contour, for section x = 88.39m: (a) mining stage 1, (b) mining stage 2, and (c) mining stage 3. 18
11. Minor principal stress contour, for section x = 82.29m: (a) mining stage 1, (b) mining stage 2, and (c) mining stage 3. 19

12(a). Local factor of safety contour plot (C =2 MPa, $\phi = 40°$) for section x = 102.87m: (a) mining stage 1, (b) mining stage 2, and mining stage 3. 21

12(b). Local factor of safety contour plot (C = 4 MPa, $\phi = 40°$) for section x = 102.87m: (a) mining stage 1, (b) mining stage 2, and mining stage 3. 22

13(a). Local factor of safety contour plot (C =2 MPa, $\phi = 40°$) for section x = 95.277m: (a) mining stage 1, (b) mining stage 2, and mining stage 3. 23

13(b). Local factor of safety contour plot (C = 4 MPa, $\phi = 40°$) for section x = 95.27m: (a) mining stage 1, (b) mining stage 2, and mining stage 3. 24

14(a). Local factor of safety contour plot (C =2 MPa, $\phi = 40°$) for section x = 88.39m: (a) mining stage 1, (b) mining stage 2, and mining stage 3. 25

14(b). Local factor of safety contour plot (C = 4 MPa, $\phi = 40°$) for section x = 88.39m: (a) mining stage 1, (b) mining stage 2, and mining stage 3. 26

15(a). Local factor of safety contour plot (C =2 MPa, $\phi = 40°$) for section x = 82.29m: (a) mining stage 1, (b) mining stage 2, and mining stage 3. 27

15(b). Local factor of safety contour plot (C = 4 MPa, $\phi = 40°$) for section x = 82.29m: (a) mining stage 1, (b) mining stage 2, and mining stage 3. 28

16. Strength/stress ratio - Hoek & Brown's empirical failure criterion (m = 3.30, s = 0.1111) for section x = 102.87m: (a) mining stage 1, (b) mining stage 2, and (c) mining stage 3. 32
17. Strength/stress ratio - Hoek & Brown's empirical failure criterion (m = 3.30, s = 0.1111) for section x = 95.25m: (a) mining stage 1, (b) mining stage 2, and (c) mining stage 3. 33
18. Strength/stress ratio - Hoek & Brown's empirical failure criterion (m = 3.30, s = 0.1111) for section x = 88.39m: (a) mining stage 1, (b) mining stage 2, and (c) mining stage 3. 34

page

19. Strength/stress ratio - Hoek & Brown's empirical failure criterion (m = 3.30, s = 0.1111) for section x = 82.29m: (a) mining stage 1, (b) mining stage 2, and (c) mining stage 3. 35

20(a). σ_x stress contour plot for section x = 102.87m: (a) mining stage 1, . . (b) mining stage 2, and (c) mining stage 3. 40

20(b). σ_x stress contour plot for section x = 95.25m: (a) mining stage 1, . . . (b) mining stage 2, and (c) mining stage 3. 41

20(c). σ_x stress contour plot for section x = 88.39m: (a) mining stage 1, . . . (b) mining stage 2, and (c) mining stage 3. 42

20(d). σ_x stress contour plot for section x = 82.29m: (a) mining stage 1, . . . (b) mining stage 2, and (c) mining stage 3. 43

21(a). σ_y stress contour plot for section x = 102.87m: (a) mining stage 1, . . (b) mining stage 2, and (c) mining stage 3. 44

21(b). σ_y stress contour plot for section x = 95.25m: (a) mining stage 1, . . . (b) mining stage 2, and (c) mining stage 3. 45

21(c). σ_y stress contour plot for section x = 88.39m: (a) mining stage 1, . . . (b) mining stage 2, and (c) mining stage 3. 46

21(d). σ_y stress contour plot for section x = 82.29m: (a) mining stage 1, . . . (b) mining stage 2, and (c) mining stage 3. 47

22(a). σ_z stress contour plot for section x = 102.87m: (a) mining stage 1, . . (b) mining stage 2, and (c) mining stage 3. 48

22(b). σ_z stress contour plot for section x = 95.25m: (a) mining stage 1, . . . (b) mining stage 2, and (c) mining stage 3. 49

22(c). σ_z stress contour plot for section x = 88.39m: (a) mining stage 1, . . . (b) mining stage 2, and (c) mining stage 3. 50

22(d). σ_z stress contour plot for section x = 82.29m: (a) mining stage 1, . . . (b) mining stage 2, and (c) mining stage 3. 51

TABLE

1. Material properties of geological formations used for modelling study . . . 9

1.0 INTRODUCTION

A cooperative study program on mine stability evaluation was initiated in 1985 involing Niobec Mines Ltd., Centre de Recherches Minérales, Quebec, and the Mining Research Laboratories(MRL) of CANMET. The present report describes Part III studies of the program. The program was structured to meet both the ground control information requirements of Niobec Mines Ltd. and the broader ground control interests of its two partners. The objectives of the program are indicated below:

(a) to contribute to the development of a geomechanical data-base on the physical and mechanical properties of mine rocks;

(b) to determine the field stresses at the mine, and to design and test instruments to monitor stress changes as mining progresses;

(c) to assess the regional and local stability of the mine structure by means of numerical simulation; and

(d) to provide design guidelines for mine design and ground control for use by mine personnel.

Centre de Recherches Minérales assumed responsibility for carrying out tasks essential to achieving objective (a). The Mining Research Laboratories assumed responsibility for carrying out tasks essential to achieving objectives (b) through (d). In this regard, in 1986 MRL carried out in situ stress determinations to provide input data on far field stresses for use in numerical analysis studies. As well, mining induced stress changes were monitored in T213-13 pillar and in the vicinity of C-203-15 stope on the 850 level. MRL strain rings were used.

In this Part III study, the stability of S-L-102-17 sill pillar was analysed using three dimensional finite element techniques. In addition, the effect of a partial removal of S-L-102-17 sill pillar on the overall stope/pillar stability was also evaluated using both Drucker/Prager yield and Hoek & Brown's empirical failure criteria.

2.0 NIOBEC MINE

The layout of Niobec Mine and the general geological conditions encounted in the mine have been described in previous reports [1,2]. Figures 1 and 2 show a plan view of the mine at the 300 level and a longitudinal section of the mine (157+50N), respectively. C-102-23 stope at the upper 300 level is currently under development with a planned stope span of 73m (240 ft). Stability evaluation studies of C-102-23 stope under idealized

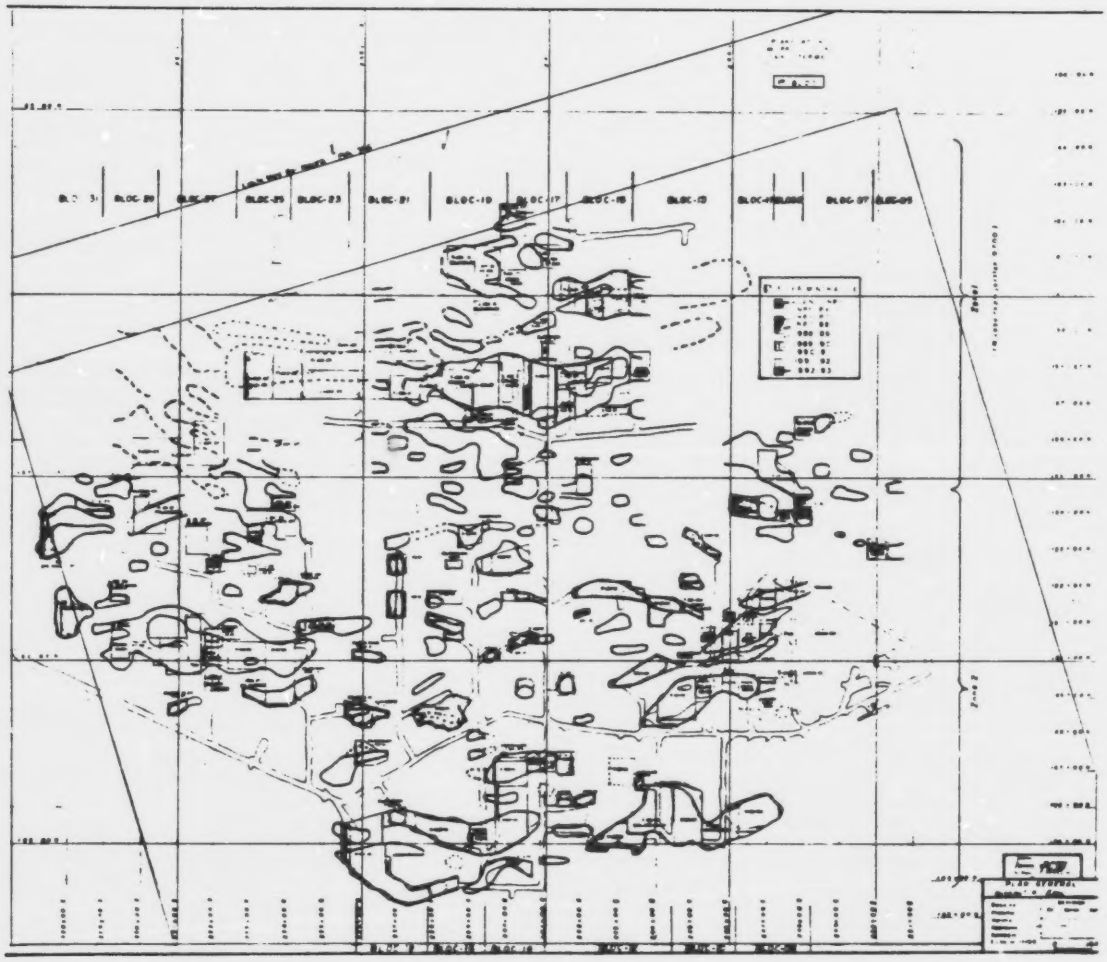

Fig. 1 A Plan View of the Niobec Mine at Level 300

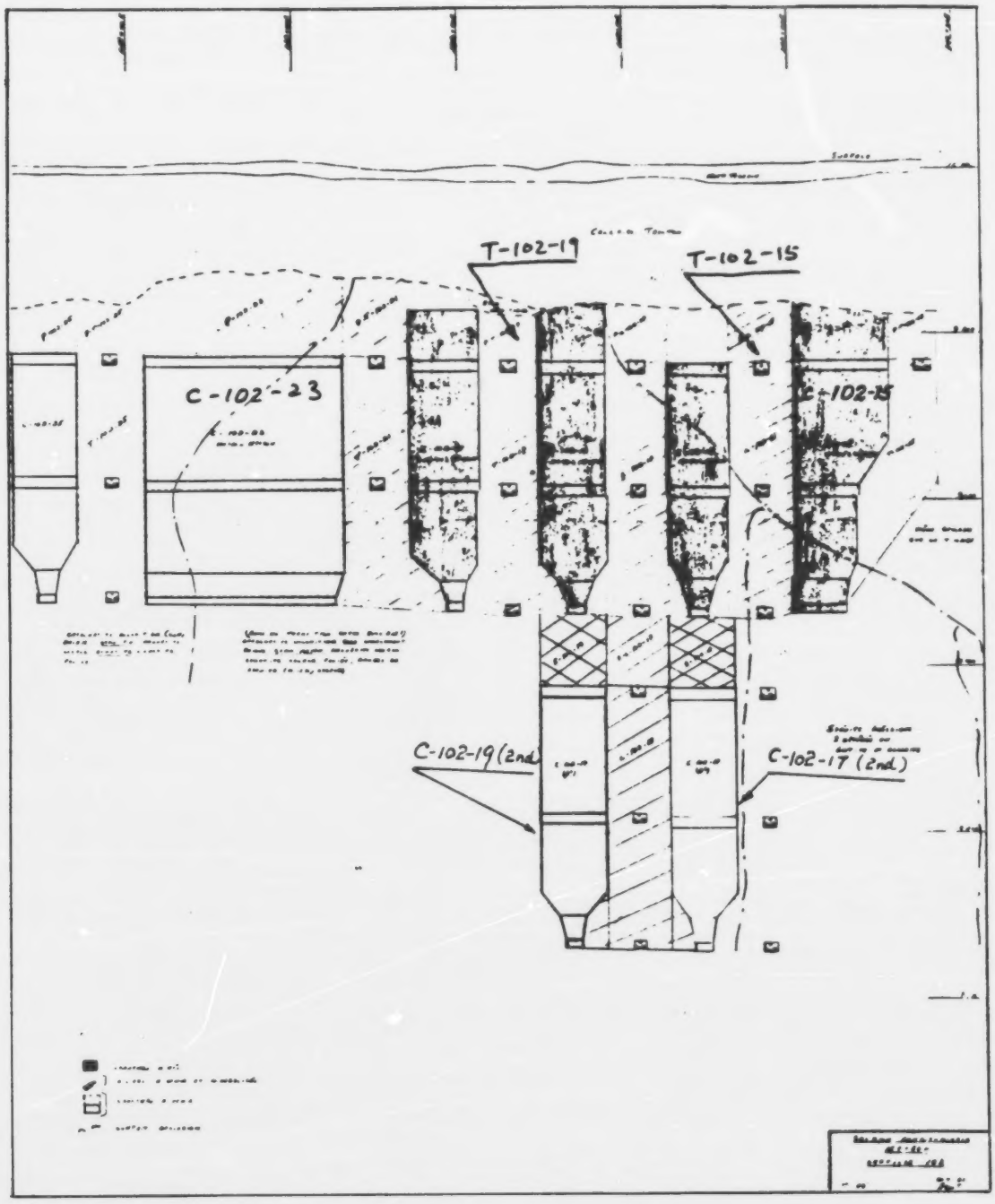

Fig. 2 A Longitudinal Section 157 + 50N of Niobec Mine

loading conditions were previously completed [1,2]. The studies indicate that stope C-102-23 could be mined without major stability problemss. However, tensile stresses could cause localized failure in the stope walls and pillars if joints are unfavorably oriented in relation to tensile stresses. Following completion of mining C-102-23 stope, the mine plans to mine additional stopes below the sill pillar and in time the sill pillar as well. Recovery of all pillars on the 300 level is planned. The present study was directed at evaluating the stability of sill pillar S-L-102-17, and the impact of mining stopes C-102-17 and C-102-19 (2nd level) on the stability of workings located on the 300 level. The stability of stopes C-102-23, C-102-17, and C-102-19 with partial removal of sill pillar S-L-102-17 was also examined.

2.1 3-D Niobec Mine Model

To study the stability of S-L-102-17 sill pillar, a new 3-D mine model was constructed including stopes C-102-17 and C-102-19 located at the lower level. To simplify mine geometry for modelling purposes, the mine model was constructed with openings symmetric around the centre plane of pillar L-102-17. As a result, only one quarter of the total structure had to be modelled. However, this did result in including in the model a mirror image of stope C-102-23 not shown in Fig. 2. Its inclusion, however, was justified on the basis that the resulting model would result in analytic studies providing a conservative estimate of opening stabilities.

An isometric view of the finite element model used in the study is shown in Fig. 3(a). It represents only one quarter of the mine 'block' being simulated. Three typical model cross sections with their finite element discretization are shown in Fig. 3(b) to 3(d). The model was constructed with more refined discretization in the area of the sill pillar and the stopes below the sill pillar because of the particular study interest in their stability.

The model was used to simulate the mine at the following stages of development:

Stage 1 - All stopes on the 300 level including stope C-102-23 mined.
Stage 2 - Stopes C-102-17 and C-102-19 below the sill pillar mined.
Stage 3 - Sill pillar S-L-102-17 between stopes C-102-17 and C-102-19 extracted.

Stage 1 was re-examined using this model which is slightly different from the model used in the two previous studies [1,2]. The results from stage 1 are included in this report for comparison purposes only. It should be noted that a coarser finite element discretization for the upper portion of the model (above 300 level) is used in the present model compared to the earlier model.

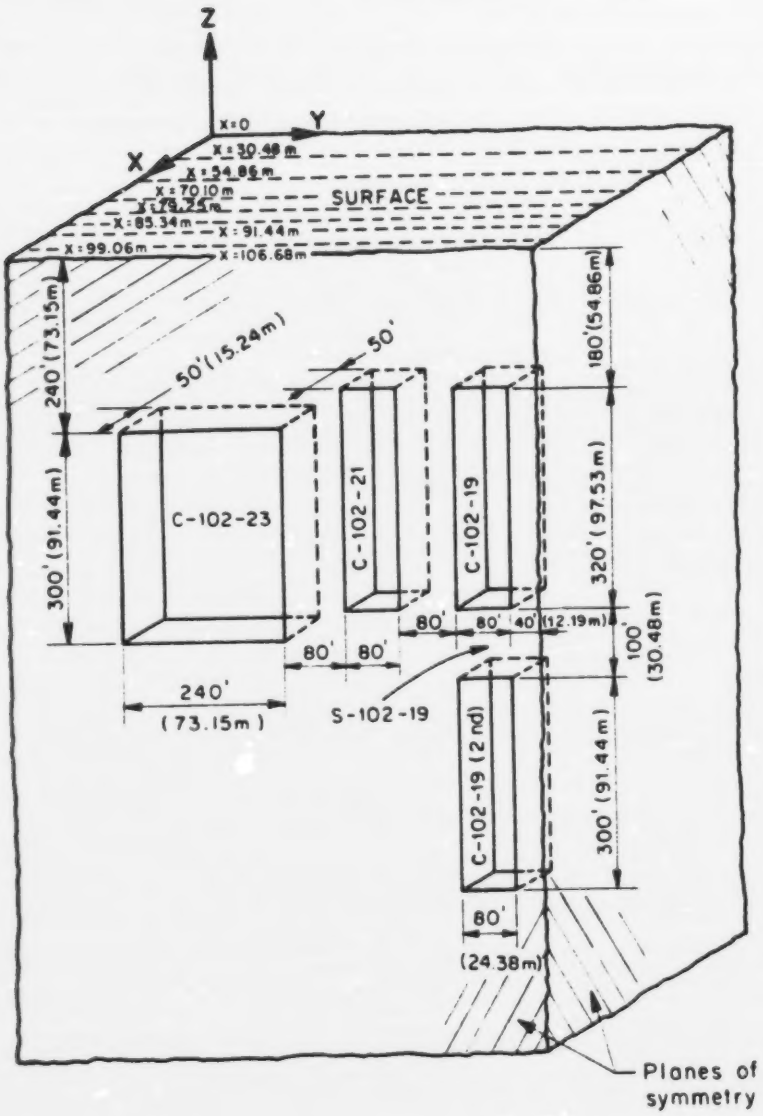

Fig. 3(a) An Isometric View of the 3-D Niobec Mine Model

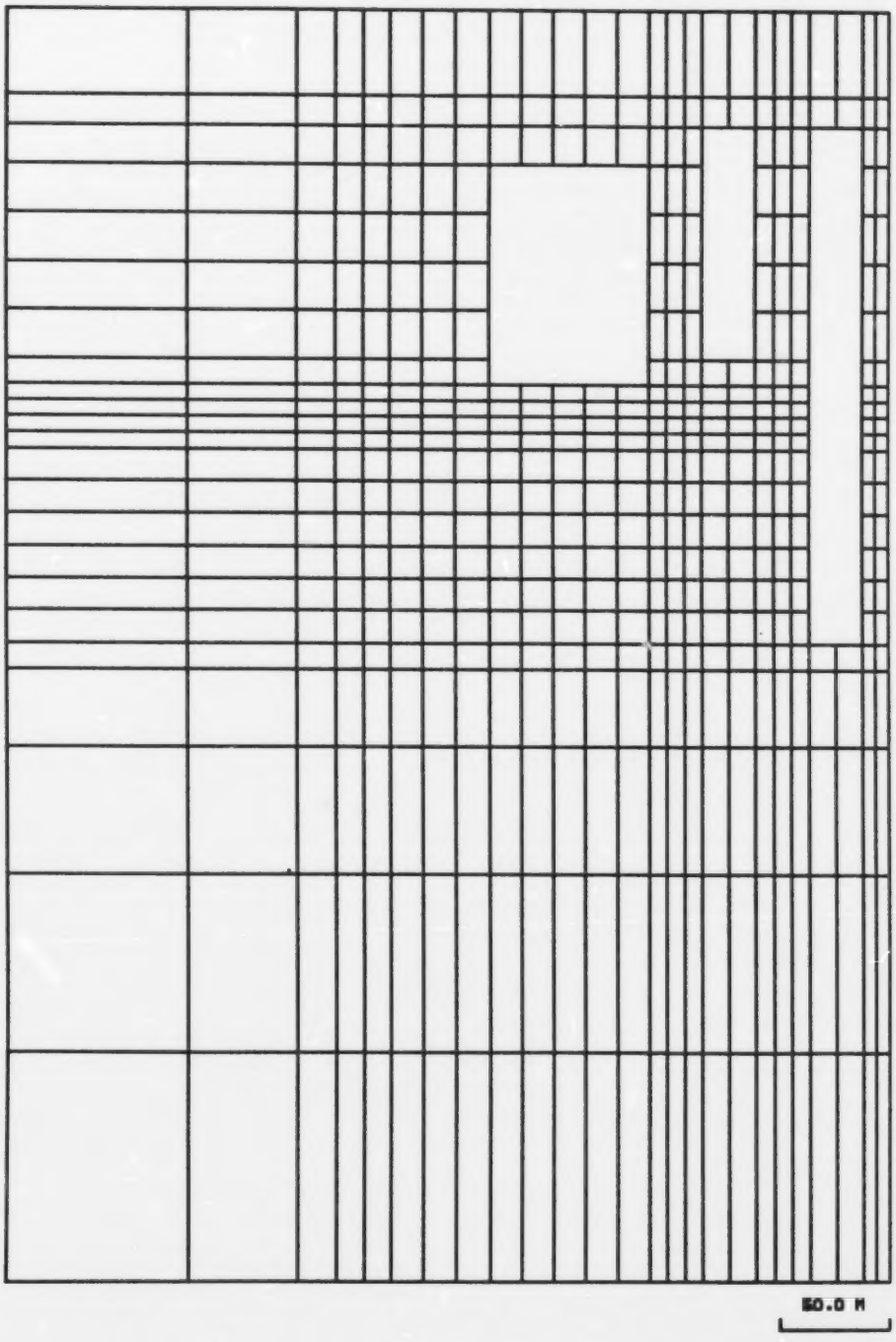

Fig. 3(b) The Finite Element Discretization for Section x = 106.68 m.

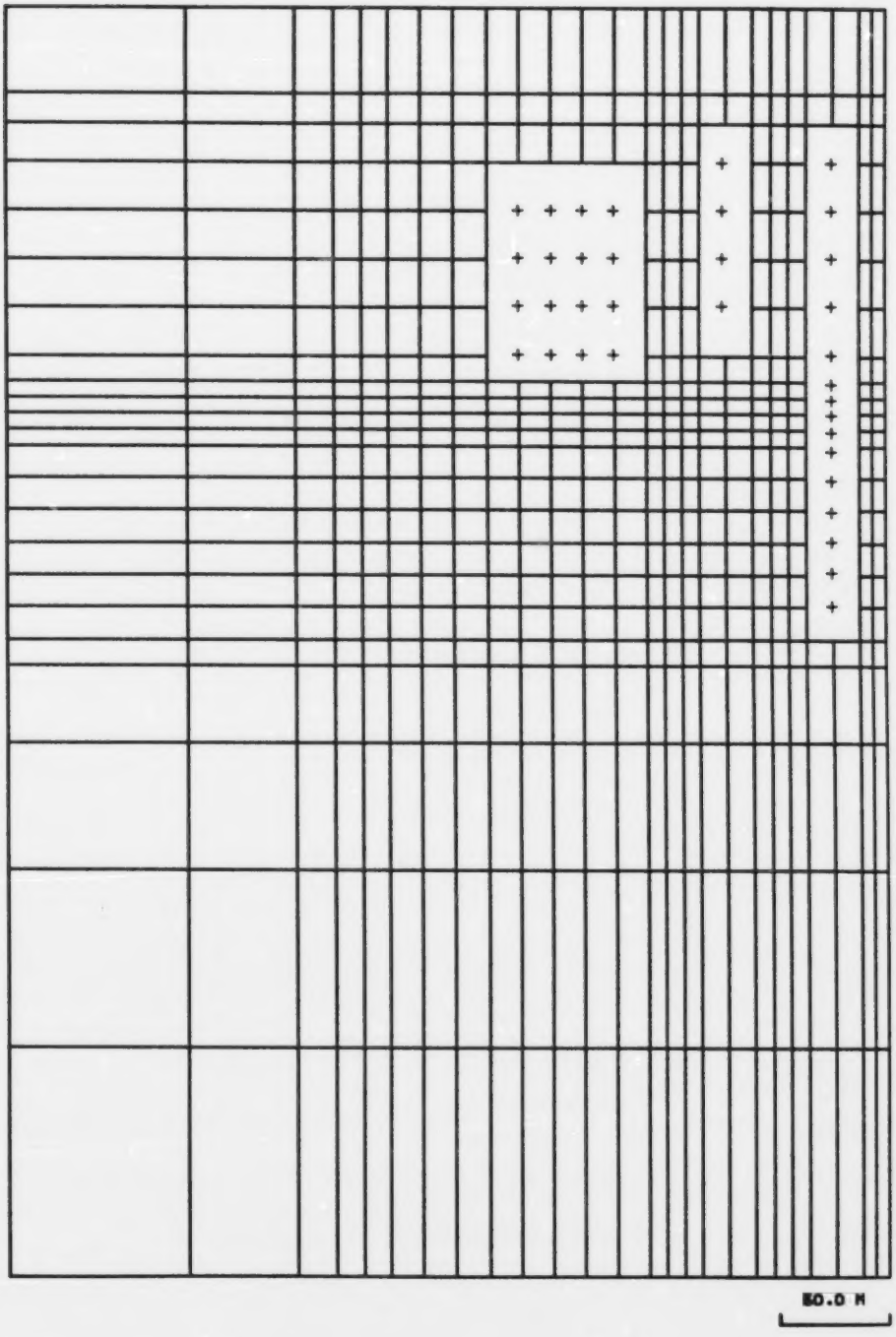

Fig. 3(c) The Finite Element Discretization for Section x = 99.09 m.

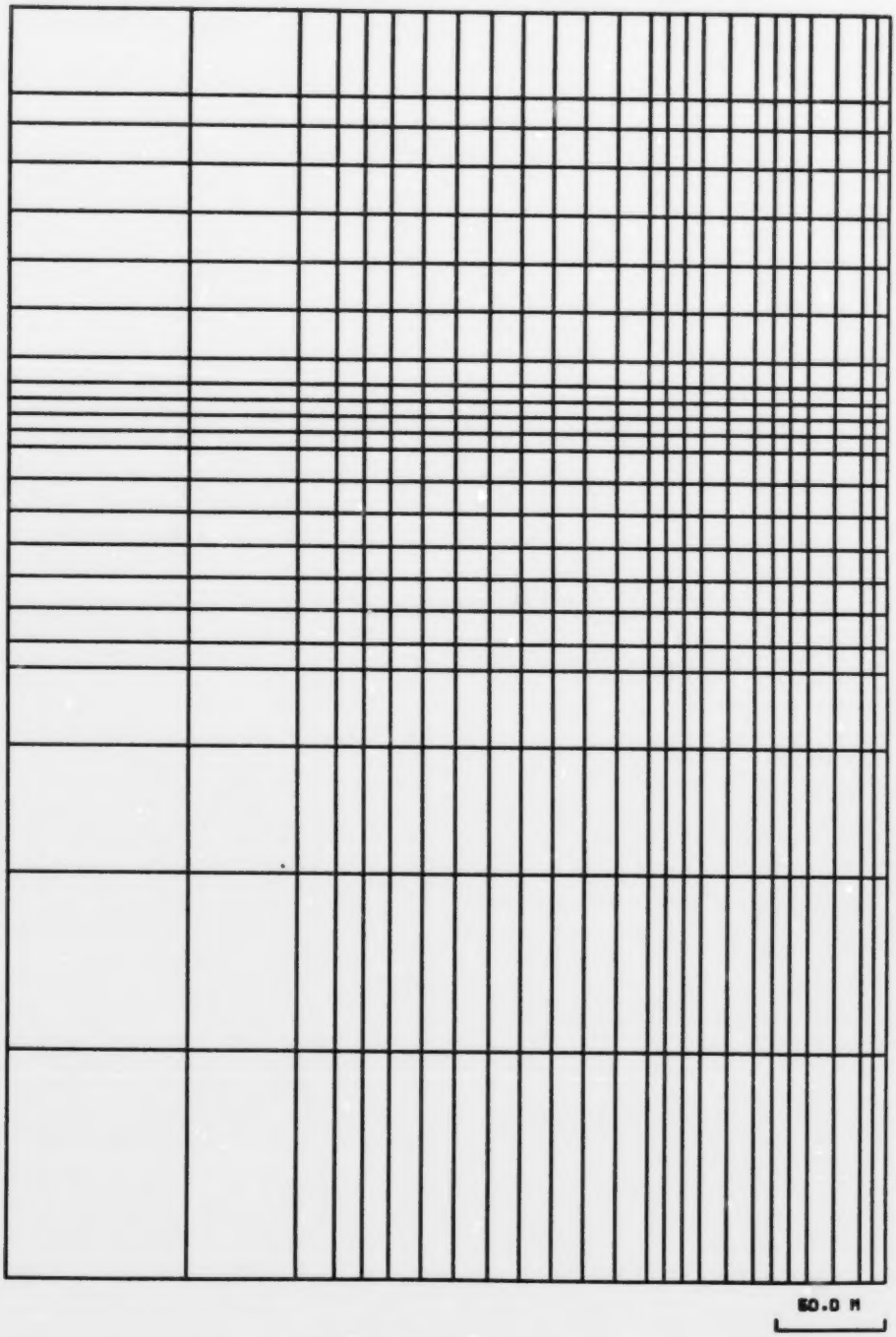

Fig. 3(d) The Finite Element Discretization for Section x = 0.0 m.

The computer model and the assumptions underlying its use in this study are the same as those used in previous studies. A basic eight-node brick element with three degrees of freedom at each node is used in the model. The model performs static, linear elastic analysis. Material properties are assumed to be isotropic. The model is capable of handling gravitational and distributed surface loads. Initial residual stresses, if known, can also be taken into consideration.

2.2 Material Properties of the Mine Rocks

The modulus of deformation, uniaxial compressive, and tensile strengths of both carbonatite and limestone formations were determined in laboratory tests [4,7]. A summary of the mechanical properties for the formations used in the study is given in Table 1.

Table 1 - Material Properties of the Geological Formations used in Modelling Study

Item	Limestone		Carbonatite (altered)		Carbonatite (intact)	
	Laboratory	Estimated*	Laboratory	Estimated*	Laboratory	Estimated*
Modulus of Deformation (MPa)	36,000	30,000	56,400	40,000	64,000	40,000
Poisson's Ratio	0.21	0.25	0.25	0.25	0.29	0.25
Uniaxial Compressive Strength (MPa)	92	45	86	45	128	45
Uniaxial Tensile Strength (MPa)	5.8	3.0	10.3	3.0	16.8	3.0
Cohesion (MPa)	10	2 - 4	17	2 - 4	25	2 - 4
Angle of Internal Friction (degrees)	36	40	50	40	51	40
Empirical Constant m	9.30	3.30	4.8	3.30	4.8	3.30
Empirical Constant s	0.04	0.1111	0.014	0.1111	0.014	0.1111
RQD's (%)	90		90		95	

* Used for modelling study;

2.3 Field Stresses

In situ stress determinations were carried out in Niobec Mine at sites located on levels 1000 and 850 [3].

In the Canadian Shield, it is known that horizontal stress is greater than vertical stress. Based on the limited stress data developed for the Niobec Mine, the following far field stress conditions were established and are referred to as Loading Case B:

$$\sigma_z = \gamma Z$$
$$\sigma_x = 1.5\sigma_z$$
$$\sigma_y = 2.0\sigma_z$$

where σ_z = *the vertical stress at depth* Z;
σ_x = *the horizontal stress in the EW direction*;
σ_y = *the horizontal stress in theNS direction*;
γ = *the unit weight of rock material*; *and*
ν = *Poisson's ratio.*

Loading case B was used to evaluate the stability of C-102-23 stope in Part II of the Niobec Mine stope stability assessment [2]. The same loading conditions were used in the present study.

3.0 RESULTS

As mentioned previously, three mining stages were simulated in this Niobec Mine model. In the first stage, all stopes on the 300 level were mined. In the second stage allowance was made for the mining of stopes C-102-17 and C-102-19 located below the 300 level sill pillar. In the third stage the simulation allowed for the partial removal of sill pillar S-L-102-17.

As mentioned earlier, finite element discretization was relatively coarse for the upper level of this new model and the stress distribution around C-102-23 stope and its adjacent areas had been examined previously [2]. The results achieved by applying the new and earlier model to C-102-23 stope under the same stress conditions were compared. As expected, the two different meshes produce different results in the roof areas of the upper level. The difference is not large and is due to the fact that large size elements were used in the roof area of the new model in order to reduce computer costs. However, the new model is capable of detecting any significant stress changes around

C-102-23 stope resulting from mining of the lower stopes or sill pillar. This is the main concerns of this study.

3.1 Stress Distribution

Figures 4, 5, 6, and 7 show, respectively, the principal stress contours resulting from all three stages of mining for sections x = 102.87m, 95.25m, 88.39m, and 82.29m. Stresses shown in Fig. 4 (section x = 102.87) represent the average stresses in the central section of the stope. Sections x = 88.39m and 82.29m are located at about 3m and 9m, respectively, into the stope walls (hangingwall or footwall). All stresses are calculated at the centroid of each element which is located at the middle plane of each 'slice'. The minor principal stress contours for the same sections are shown in Fig. 8, 9, 10, and 11. These figures provide a quick and direct comparison between stress conditions at different stages of mining. The development of tensile zones at different mining stages is shown as shaded areas in Fig. 8, 10, and 11. Tensile stresses occur along the stope walls in the centre section of stope as shown in Fig.8. Tensile zones penetrate into the stope walls in the N-S direction approximately 9m as shown in Figs. 10 and 11. The stress components in the x, y, and z directions, respectively, are shown with shaded tensile zone in Figs. 20, 21 and 22 in Appendix A.

As expected, mining of C-102-17 stope, C-102-19 stope, and sill pillar S-L-102-17 under existing far field stresses, results in the development of high compressive stress conditions around the lower portion of stopes C-102-17 and C-102-19. However, these stresses are not high enough to create zones of shear failure. Tensile stresses occur in stope walls, and along the pillars. A maximum tension of 1.9 MPa occurs in the lower portion of pillar L-102-17.

The results can be summarized as follows:

(a) Under existing stress conditions (loading case B), the effect of excavating stopes C-102-17 and C-102-19 below the sill pillar on the stability of stope C-102-23 and adjacent areas will be nominal. The largest compressive stresses occur near stope corners with a magnitude of about 22 MPa. They are not sufficiently high to cause stability problems in terms of shear failure.

(b) Tensile stress developed along the walls of C-102-23 stope (T-102-21 pillar) are relatively small. The stresses are less than 1.0 MPa. However, when sill pillar S-L-102-17 between stopes C-102-17 and C-102-19 is extracted (mining stage 3), tensile stresses are developed along most of the length of L-102-17 pillar. The maximum tensile stress is approximately 1.9 MPa, and occurs at about one-eighth of the pillar height from the pillar toe. Even though the tensile strength of

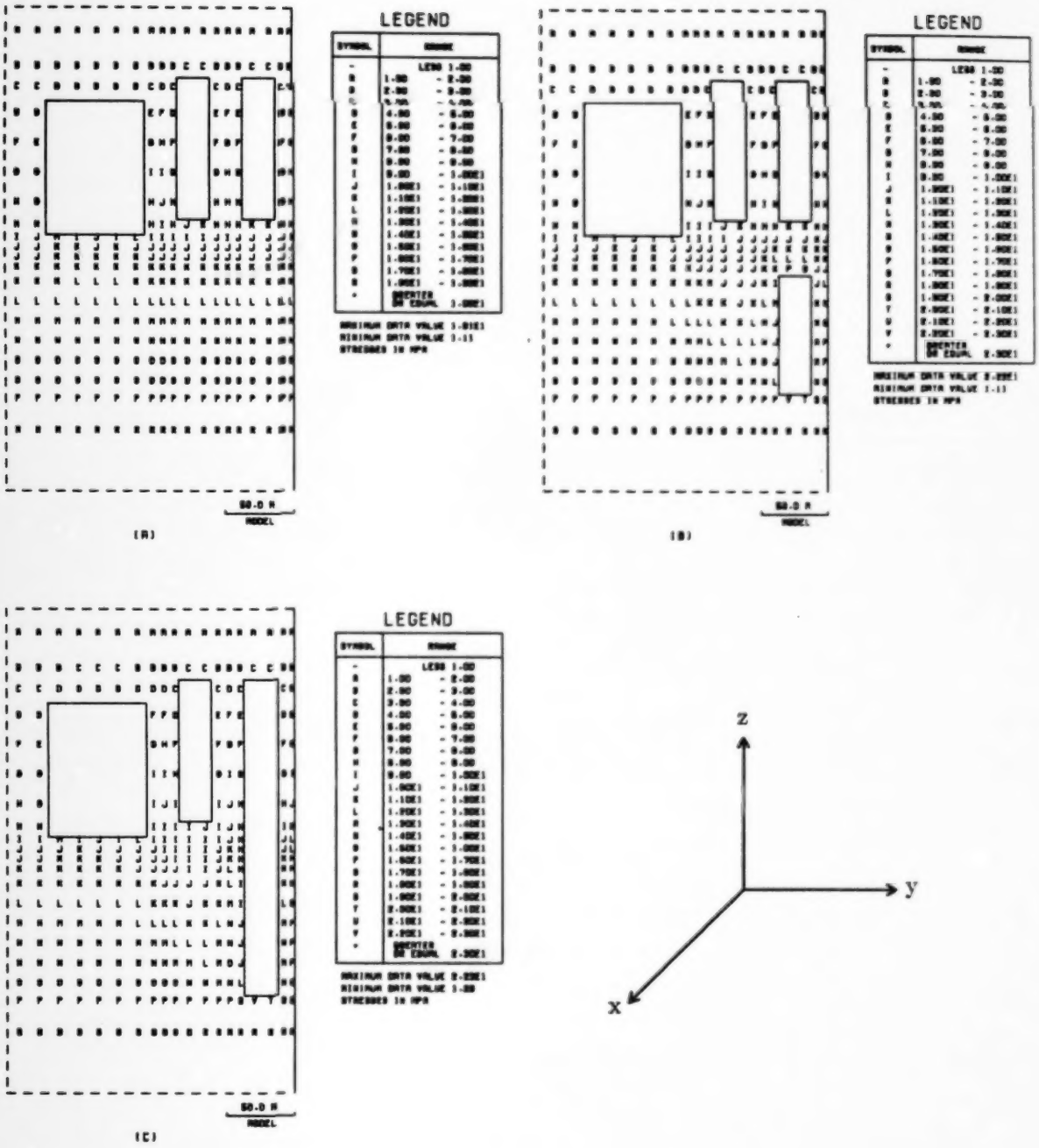

Fig. 4 Major principal stress contour plot for section x = 102.87m : (A) mining stage 1, (B) mining stage 2, and (C) mining stage 3.

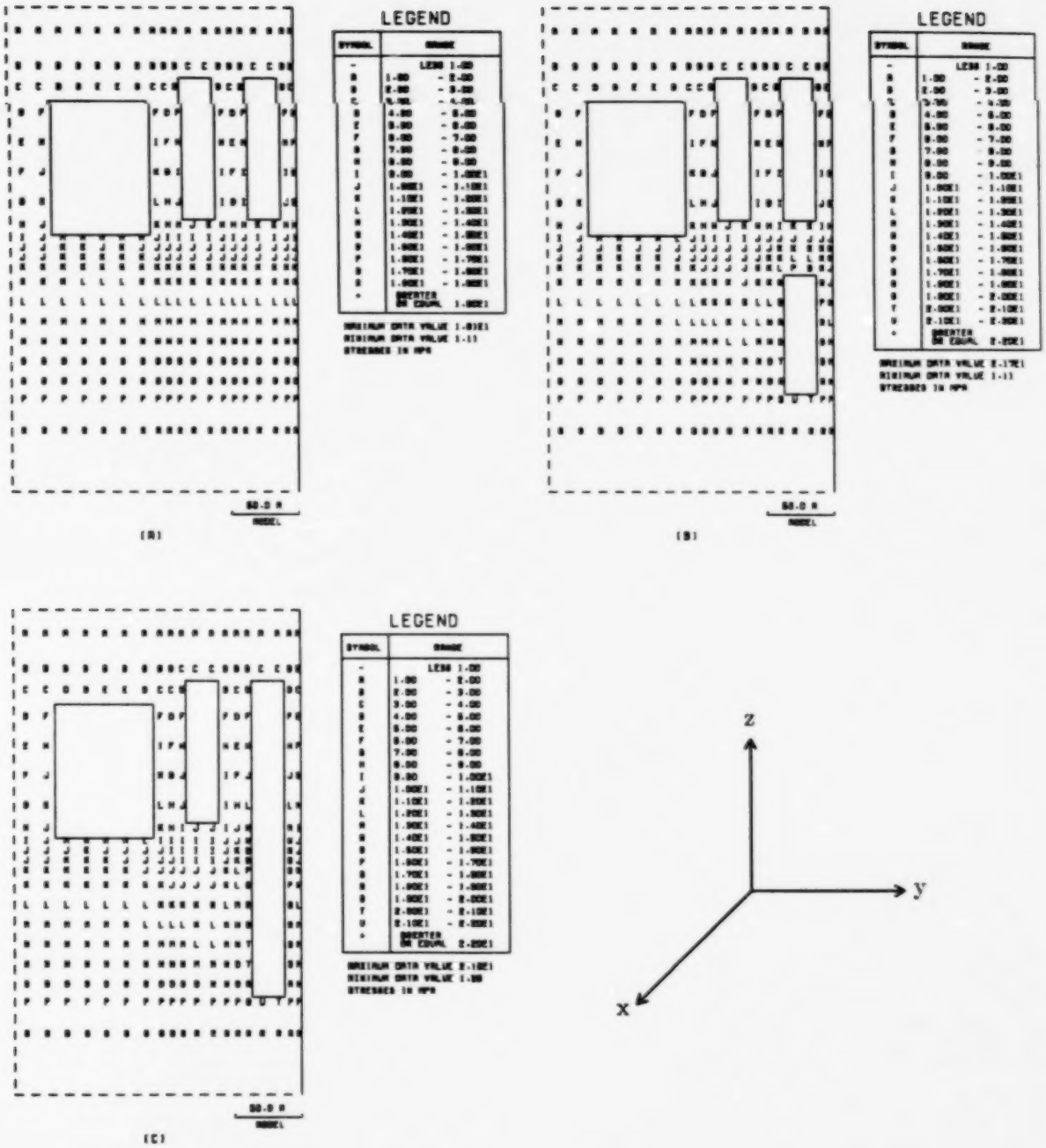

Fig. 5 Major principal stress contour plot for section x = 95.25m : (A) mining stage 1, (B) mining stage 2, and (C) mining stage 3.

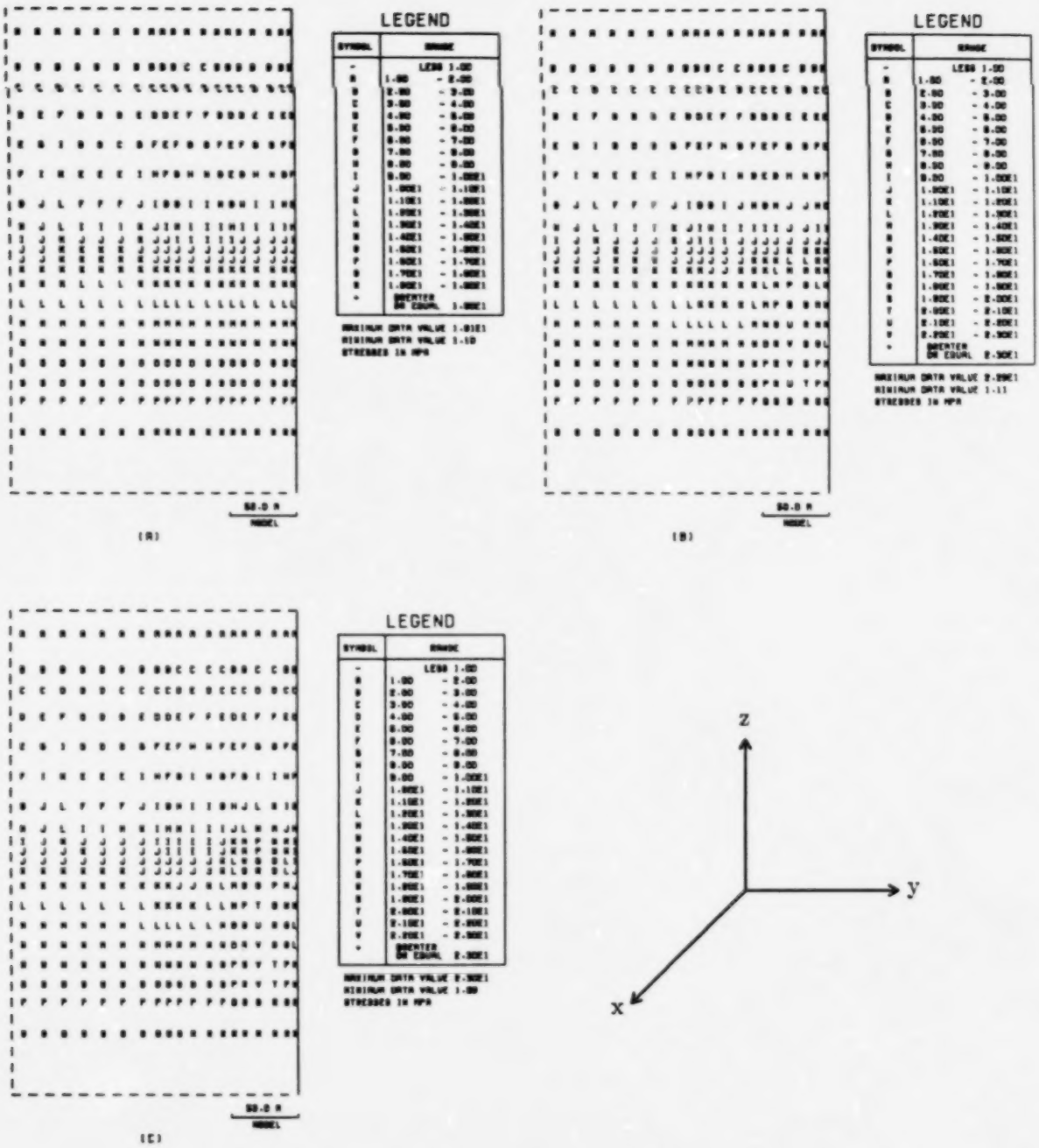

Fig. 6 Major principal stress contour plot for section x = 88.39m : (A) mining stage 1, (B) mining stage 2, and (C) mining stage 3.

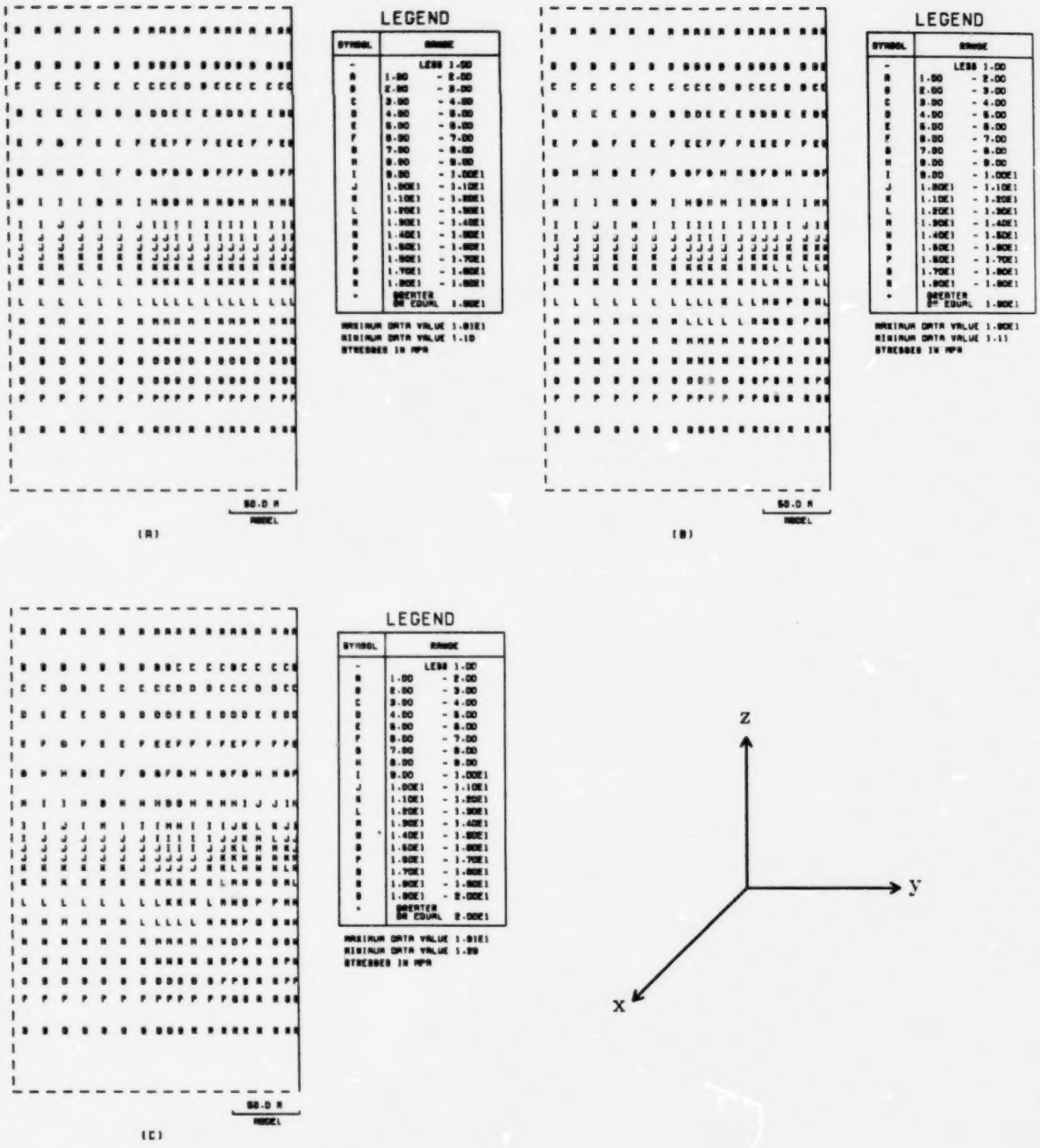

Fig. 7 Major principal stress contour plot for section x = 82.29m : (A) mining stage 1, (B) mining stage 2, and (C) mining stage 3.

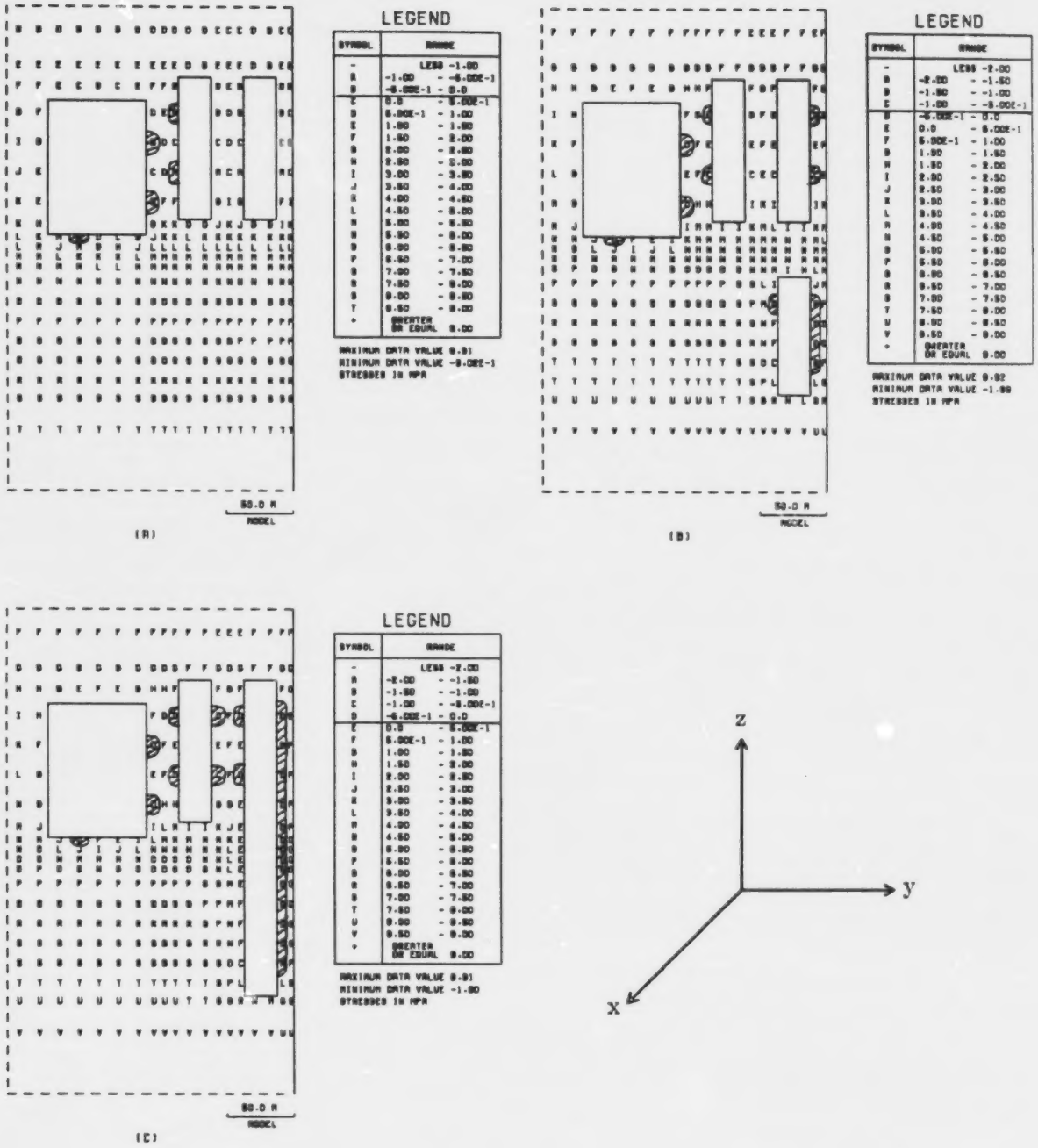

Fig. 8 Minor principal stress contour plot for section x = 102.87m : (A) mining stage 1, (B) mining stage 2, and (C) mining stage 3.

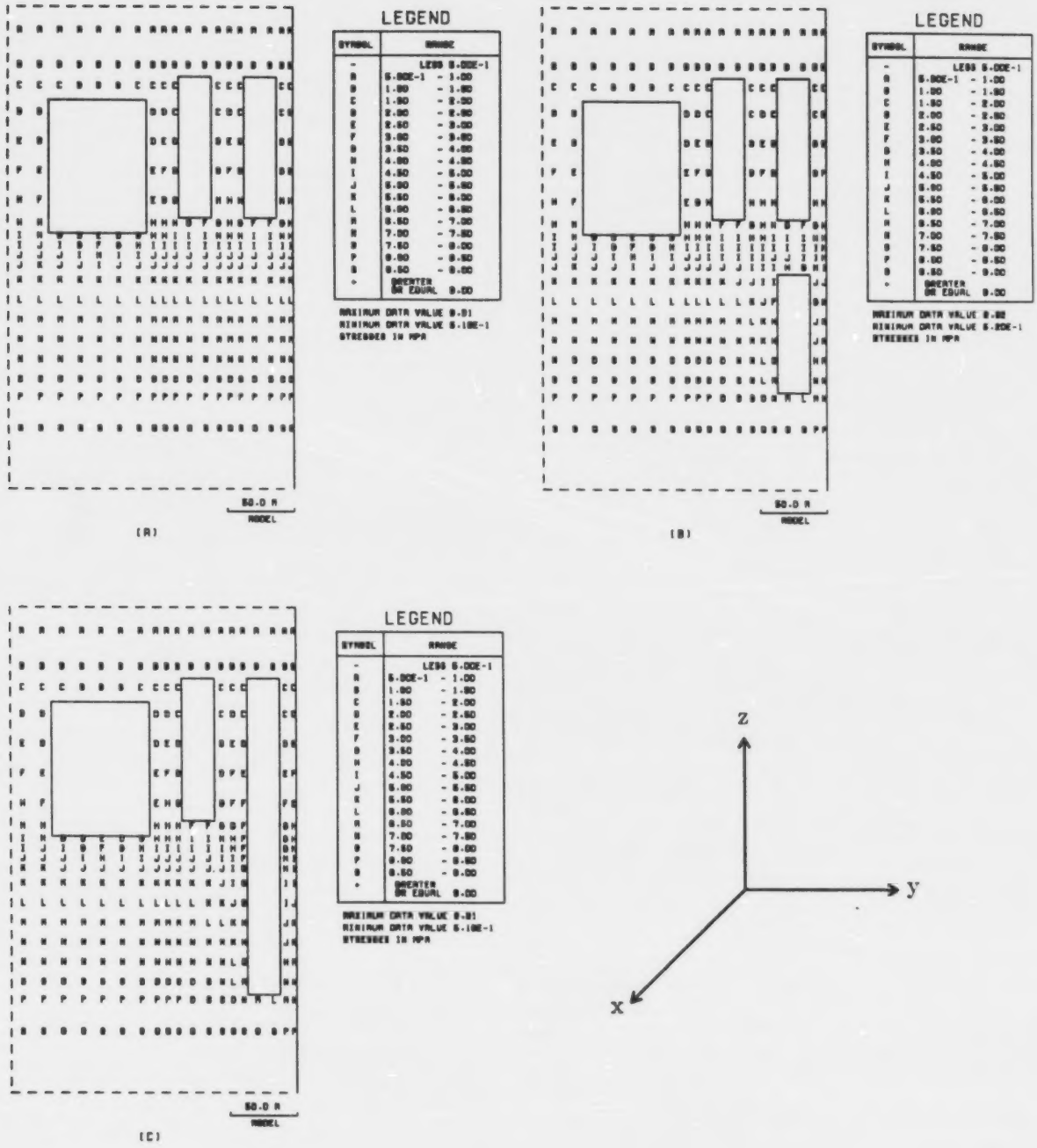

Fig. 9 Minor principal stress contour plot for section x = 95.25m : (A) mining stage 1, (B) mining stage 2, and (C) mining stage 3.

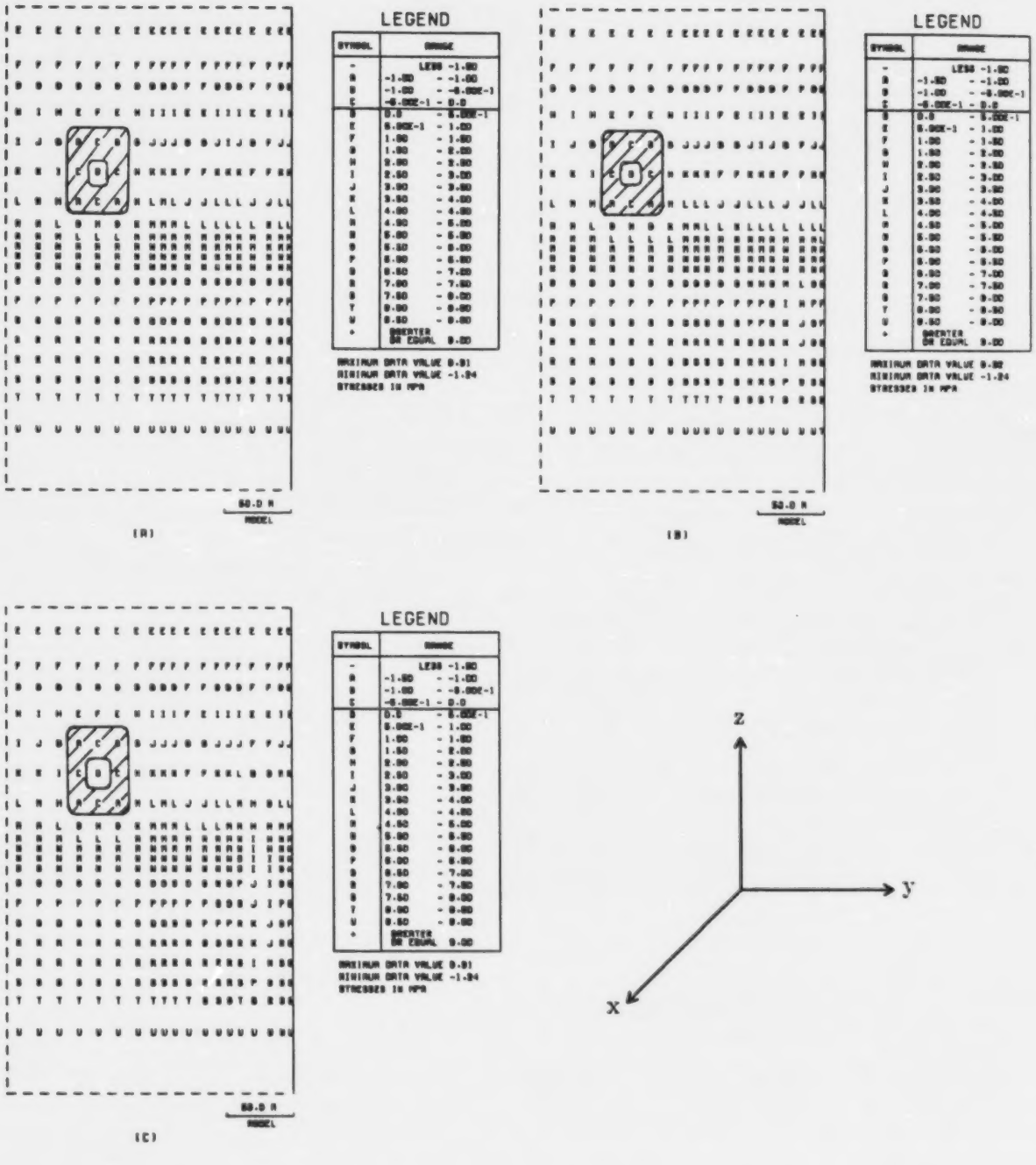

Fig. 10 Minor principal stress contour plot for section x = 88.39m : (A) mining stage 1, (B) mining stage 2, and (C) mining stage 3.

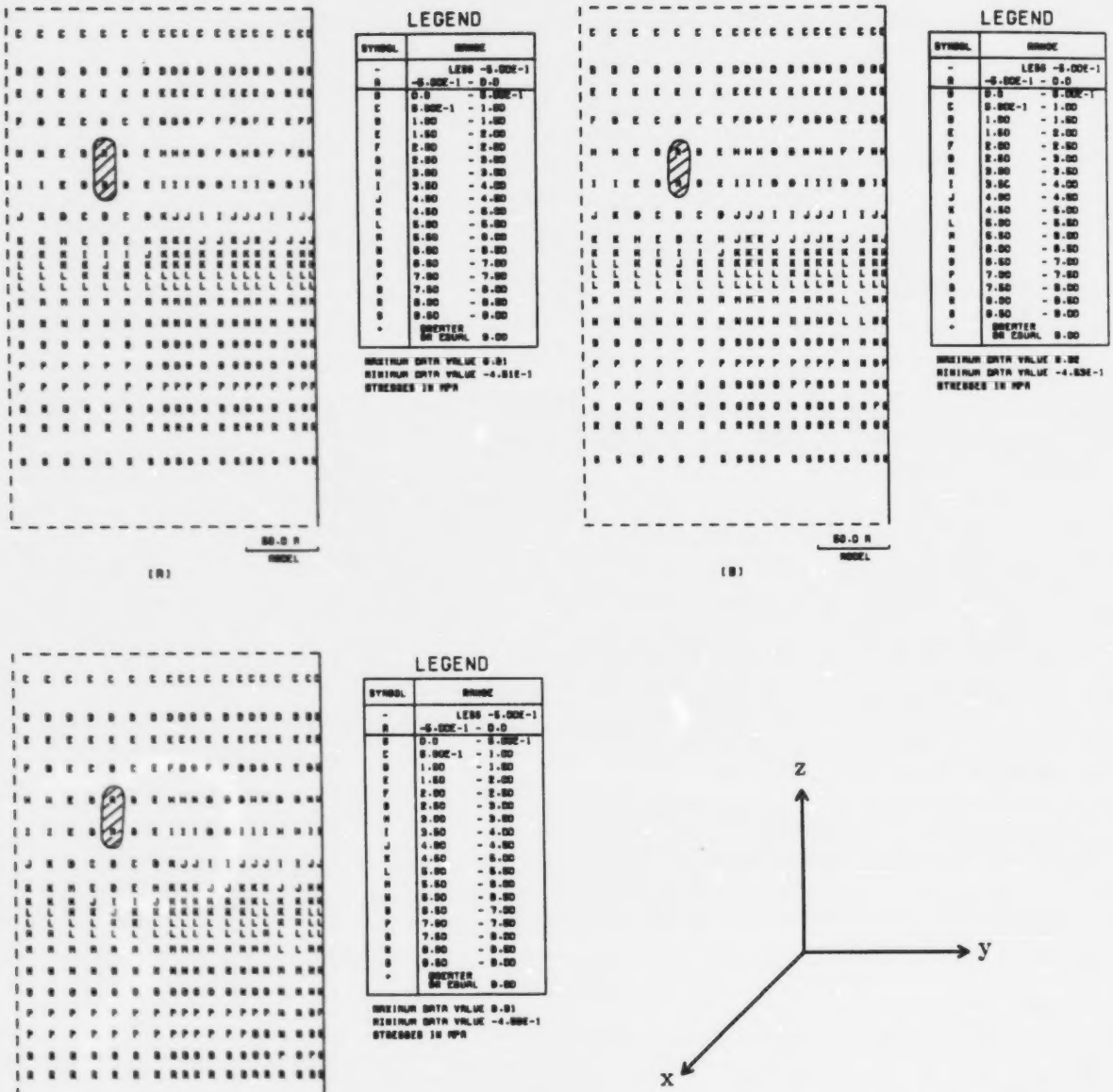

Fig. 11 Minor principal stress contour plot for section x = 82.29m : (A) mining stage 1, (B) mining stage 2, and (C) mining stage 3.

carbonatite is estimated at 5 - 10 MPa, if joints are unfavorably orientated, pillar stability could be a problem. Since the pillar is only 24m wide, consideration should be given to ensuring its integrity. In other words, the sill pillar seems to be providing important structural support and should be maintained until mining on the upper level is completed.

3.2 Potential Failure Areas

It is difficult to find a realistic failure criterion for a rock mass surrounding an underground excavation, since the stability of the rock in the immediate vicinity of underground openings is related to pre-existing discontinuities and fractures induced in the rock by blasting, and drilling processes, etc. For the purpose of underground excavation design, the failure criterion should describe the response of the rock mass under different stress conditions (from uniaxial tensile to triaxial compression). It should also be capable of predicting the influence of discontinuities on rock mass behaviour. Back analysis seems to be a rational approach and should be considered in any future study.

No one criterion is capable of predicting potential ground failure for all types of rock. The Drucker/Prager yield criterion takes into account triaxial stress conditions but fails to consider any tensile failure. In recent years, Hoek and Brown's empirical failure criterion appears to be gaining popularity in rock mechanics applications. Although it does not take into consideration intermediate principal stress, it does take into account rock mass quality and both shear and tensile modes of failure.

3.2.1 Drucker/Prager Yield Criterion

As an indicator for potential failure around stopes, the strength/stress ratio or the local factors of safety (LFS) in terms of the Drucker/Prager yield function have been calculated for the four sections under consideration, i.e., for the planes x = 102.87m, 95.25m, 88.39m and 82.29m. The strength/stress ratio or LFS contour maps are shown in Figs. 12, 13, 14 and 15. The Drucker/Prager yield criterion takes all three principal stresses into consideration. The detailed calculation of LFS or strength/stress ratio using the Drucker/Prager yield function is given in Appendix A of a previous report [1].

The material constants used in this analysis were $C = 2MPa$ and $\phi = 40°$, where C is the cohesive strength and ϕ the angle of internal friction. A number of areas with factors of safety between 1.0 - 1.50 were outlined as shown in Figs. 12(a), 12(b), 13(a), 14(a), 14(b) and 15(a). Only one area occured where LFS was ≤ 1.0 as shown by the shaded area in Fig. 12(a). This area occurred in the lower portion of L-102-17 pillar. The values used in the study for cohesive strength C and angle of internal friction ϕ,

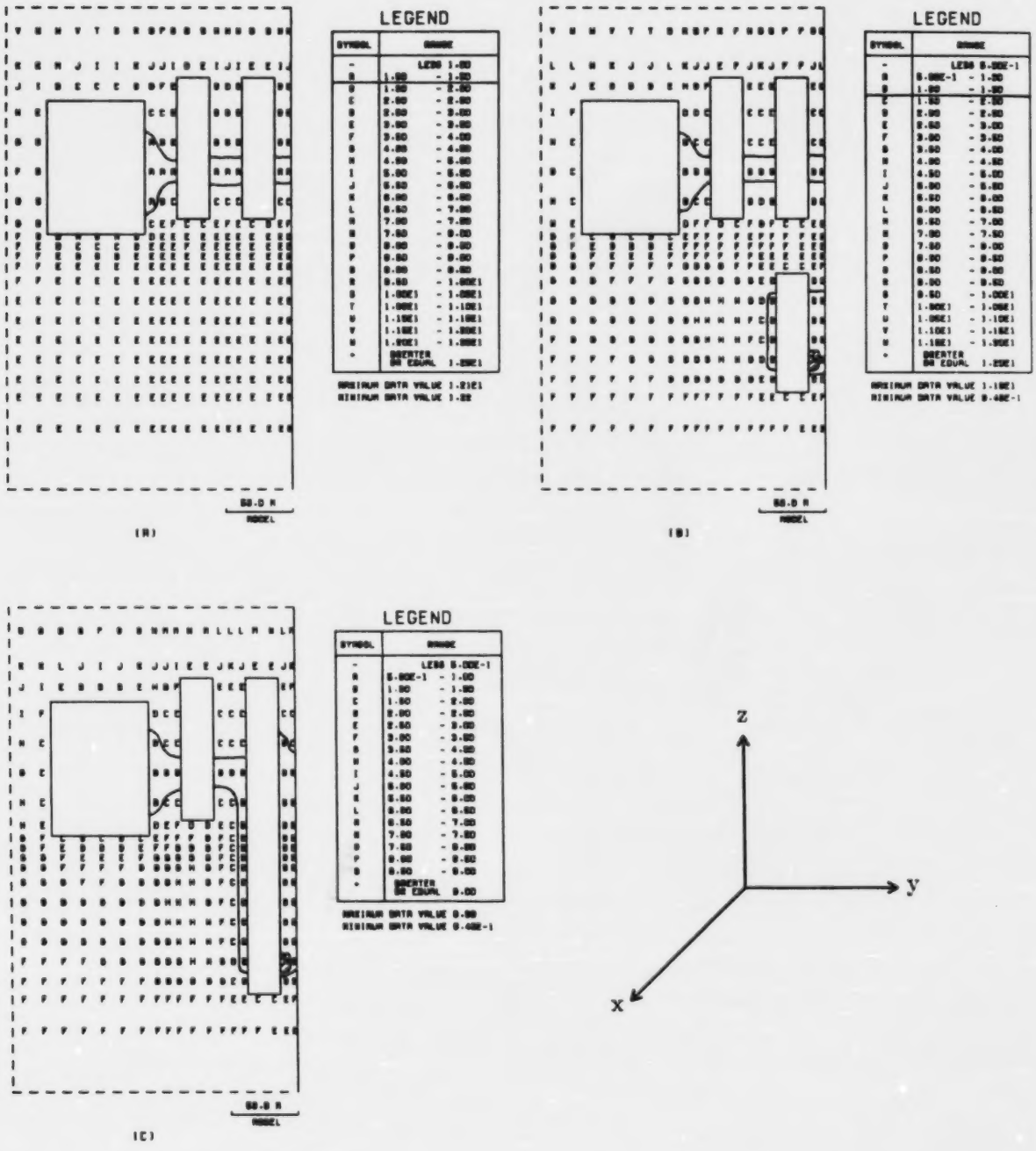

Fig. 12(a) Local factor of safety contour plot (C=2 MPa, $\phi = 40°$) for section x = 102.87m: (A) mining stage 1, (B) mining stage 2, and (C) mining stage 3.

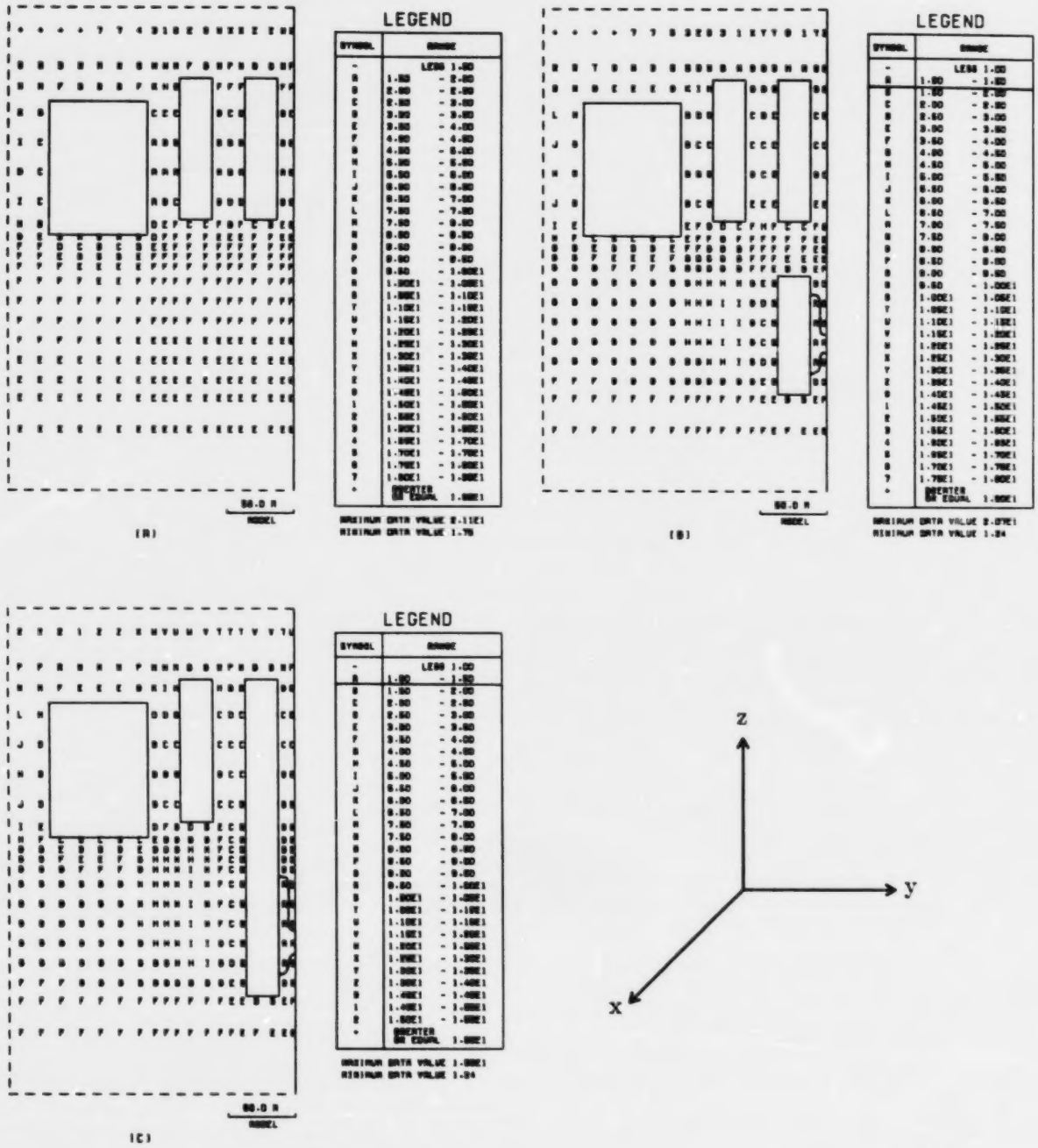

Fig. 12(b) Local factor of safety contour plot (C=4 MPa, $\phi = 40°$) for section x = 102.87m: (A) mining stage 1, (B) mining stage 2, and (C) mining stage 3.

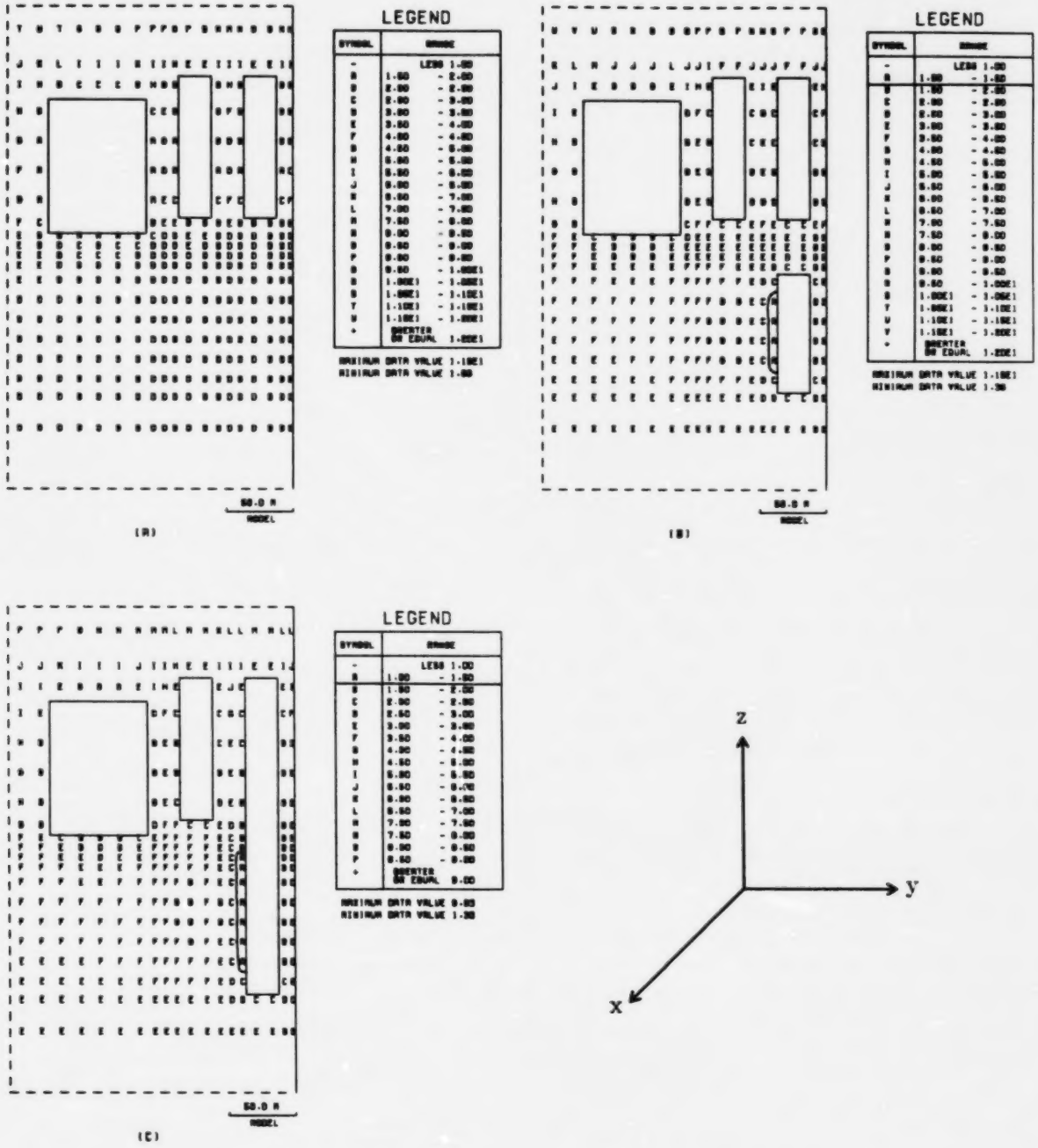

Fig. 13(a) Local factor of safety contour plot (C=2 MPa, $\phi = 40°$) for section x = 95.27m: (A) mining stage 1, (B) mining stage 2, and (C) mining stage 3.

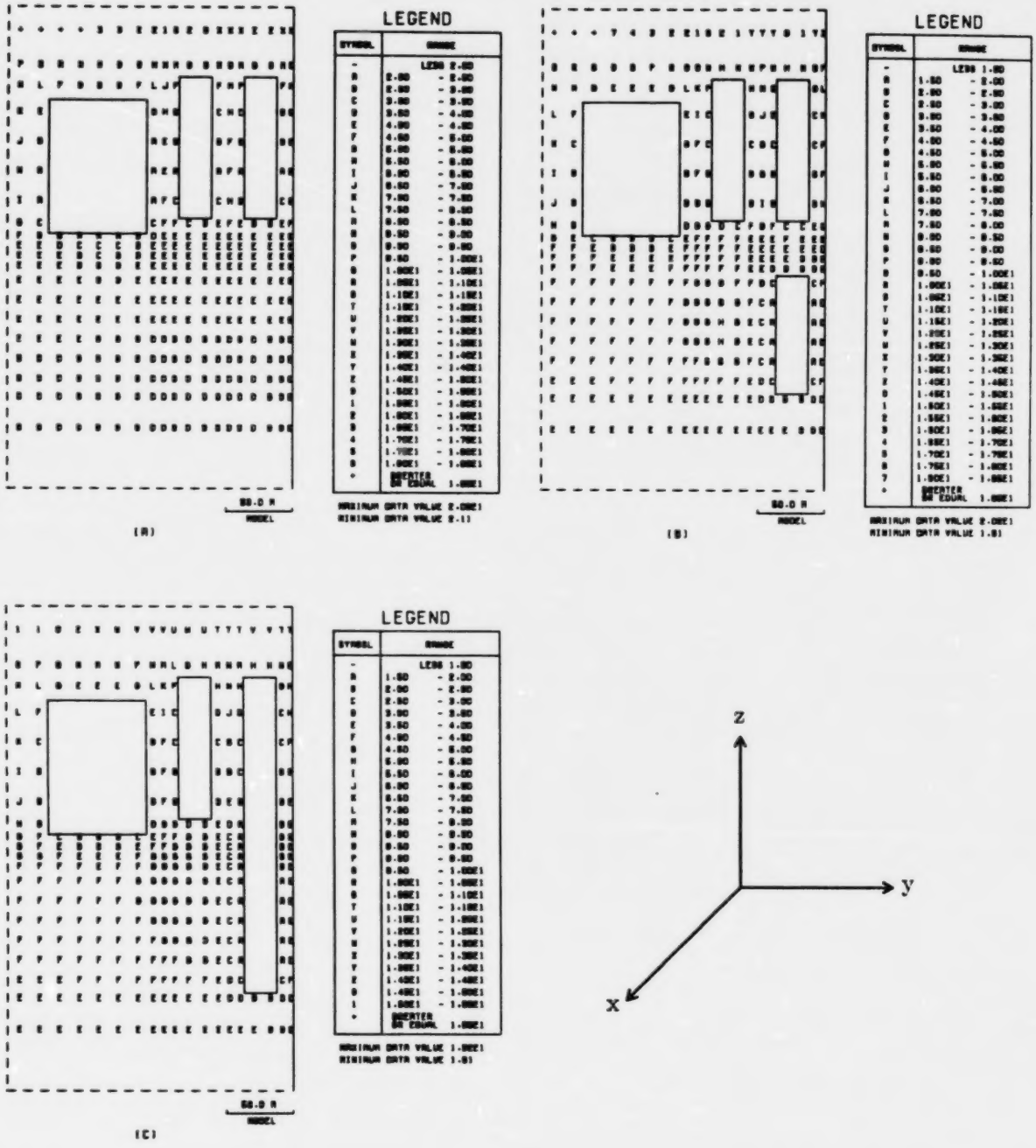

Fig. 13(b) Local factor of safety contour plot (C=4 MPa, $\phi = 40°$) for section x = 95.27m: (A) mining stage 1, (B) mining stage 2, and (C) mining stage 3.

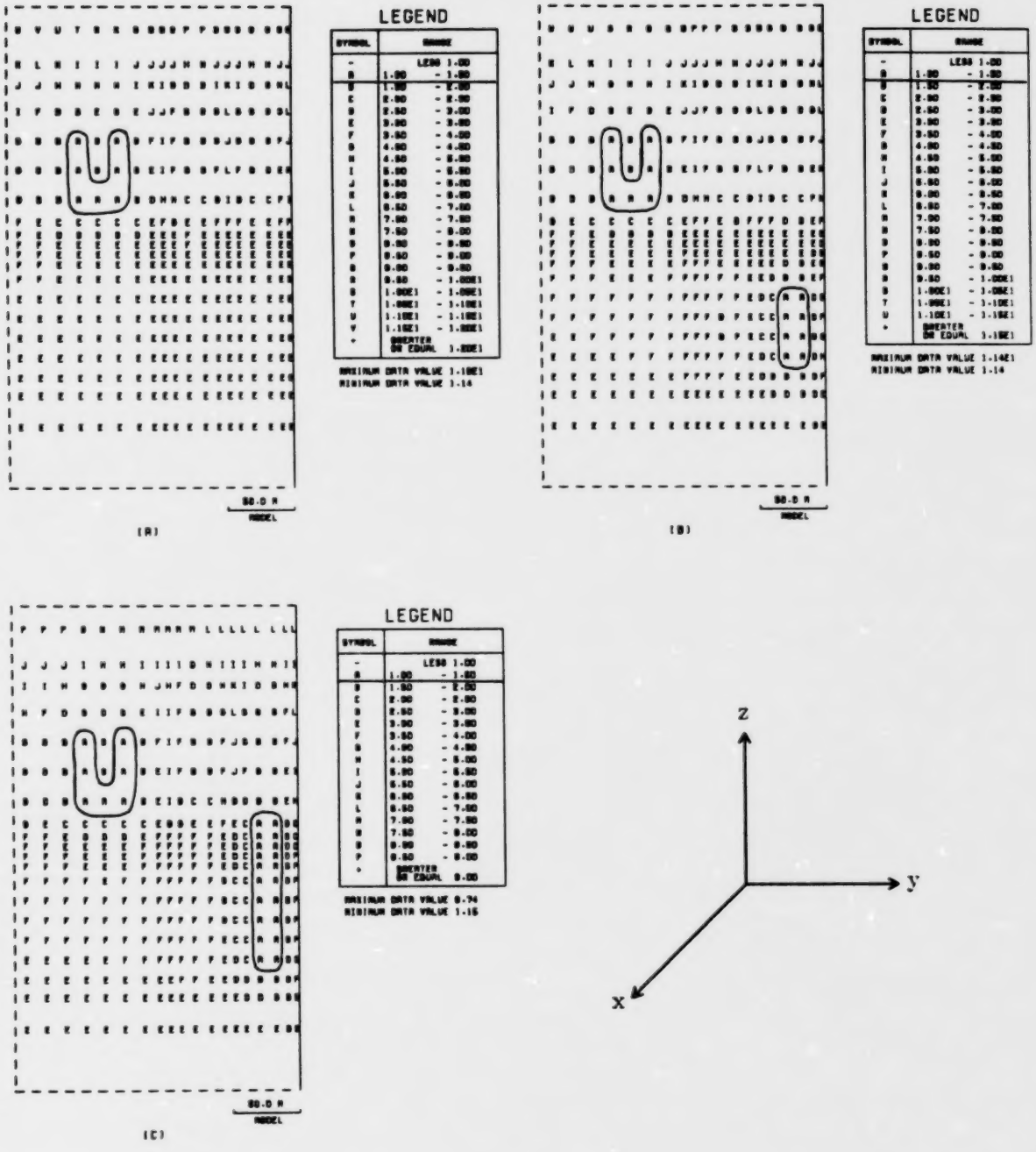

Fig. 14(a) Local factor of safety contour plot (C=2 MPa, $\phi = 40°$) for section x = 88.39: (A) mining stage 1, (B) mining stage 2, and (C) mining stage 3.

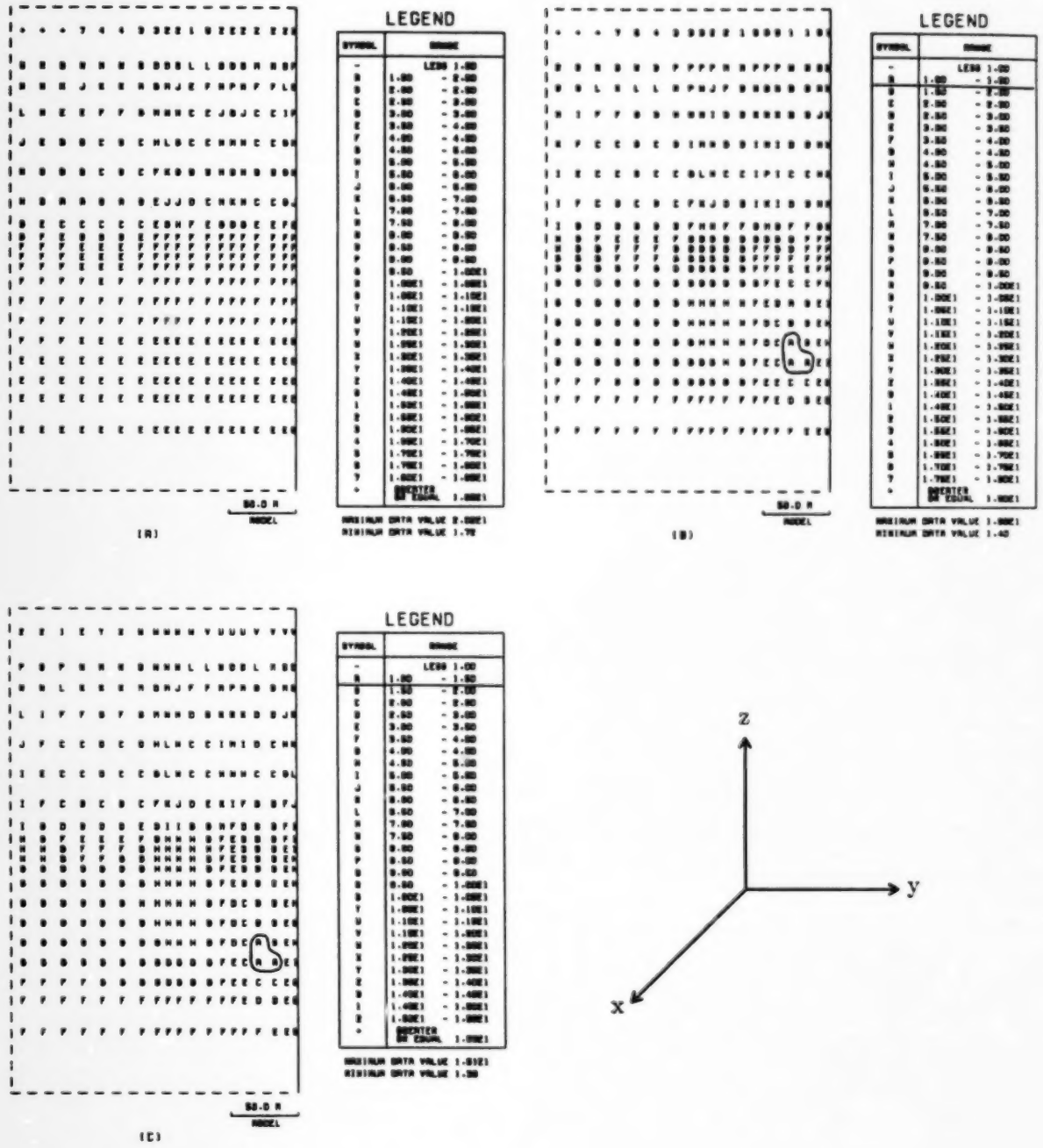

Fig. 14(b) Local factor of safety contour plot (C=4 MPa, $\phi = 40°$) for section x = 88.39m: (A) mining stage 1, (B) mining stage 2, and (C) mining stage 3.

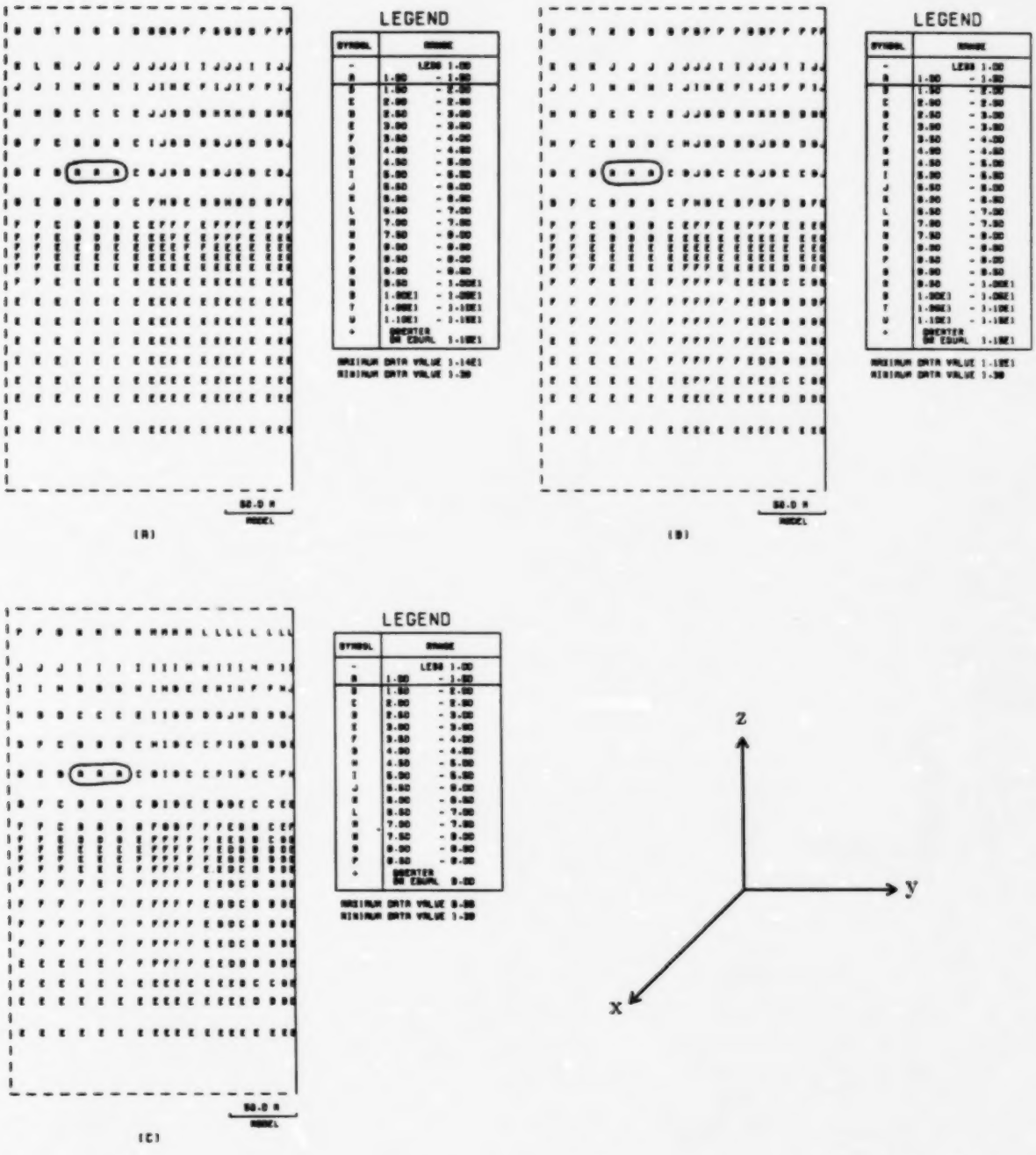

Fig. 15(a) Local factor of safety contour plot (C=2 MPa, $\phi = 40°$) for section x = 82.29m: (A) mining stage 1, (B) mining stage 2, and (C) mining stage 3.

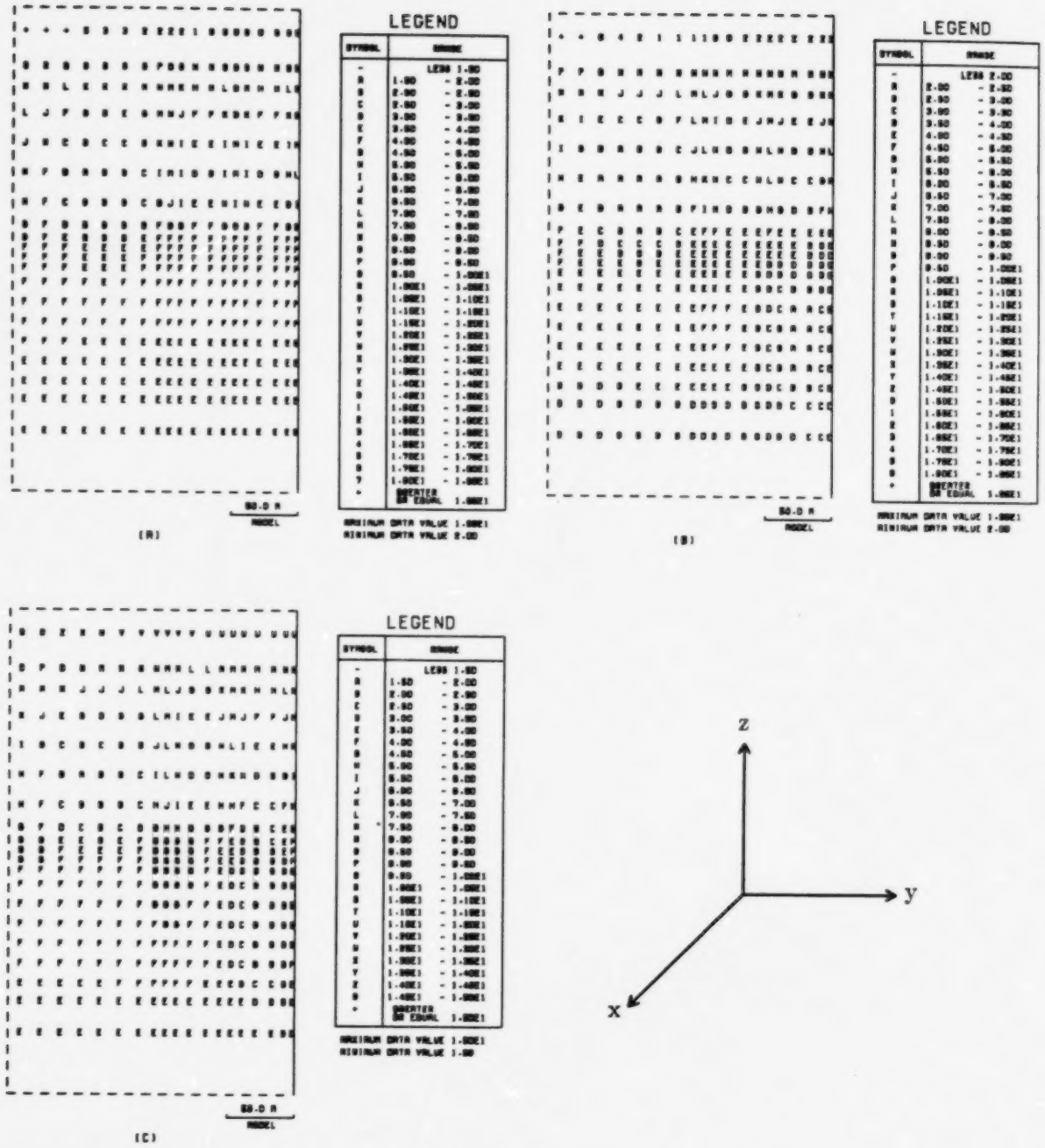

Fig. 15(b) Local factor of safety contour plot (C=4 MPa, $\phi = 40°$) for section x = 82.29m: (A) mining stage 1, (B) mining stage 2, and (C) mining stage 3.

2 MPa and 40° respectively, may be too conservative. An additional study was carried out using $C = 4MPa$, with $\phi = 40°$. The minimum LFS increased from 0.95 to 1.24.

The laboratory determined compressive strengths for the intact and altered carbonatite are 130 MPa and 90 MPa, respectively [4]. No procedures presently exit to estimate in situ rock mass strength based on laboratory tests. A worst case scenario would be a concentration of altered carbonatite rock in the lower level of the Niobec Mine. If we apply a reduction factor of 2 to the strength of the intact samples, then, the in-situ compressive strength of the altered carbonatite would be 45 MPa. Assuming the material obeys the Coulomb criterion of brittle failure, then the compressive strength, σ_u, can be related to the rock cohesive strength and angle of internal friction by the equation: $\sigma_u = 2C(1 + \sin\phi)/(1 - \sin\phi)$. For altered carbonatite $\sigma_u = 45MPa$, and $\phi = 40°$ and the cohesive strength of carbonatite is estimated as 8.7 MPa. Therefore, a value of C = 4 MPa used in shear failure analysis seems to be reasonable and would provide conservative estimate of structural performance. On this basis, the local factors of safety calculated for the pillars and stope walls appear to be more than adequate. Therefore, no imminent shear failure is anticipated. If failure should occur, it would be localized tensile failure rather than shear failure.

3.2.2 Hoek and Brown's Empirical Failure Criterion

Another indicator for failure is based on Hoek and Brown's empirical failure criterion. Assuming that the intermediate principal stress has no influence on failure, the equation relating the principal stresses at failure is given by [5]:

$$\sigma_1 = \sigma_3 + \sqrt{m\sigma_c\sigma_3 + s\sigma_c^2} \qquad (1)$$

where σ_1, σ_3 = *the major and minor principal stresses at failure,*

σ_c = *the uniaxial compressive strength of the intact rock material in the specimen,*

m, s = *constants depend upon the properties of the rock and upon the extent to which it has been broken before being subjected to the stresses* σ_1 *and* σ_3. *For intact rock* $s = 1$, *for previously over stressed* $s < 1$, *and for jointed and broken rock sample s decreases to a limiting value of zero.*

The uniaxial compressive strength, σ_u, and the uniaxial tensile strength, σ_t, of the rock specimen (rock mass) can be related to the uniaxial compressive strength of the intact rock material in the specimen [5]:

$$\sigma_u = \sqrt{s\sigma_c^2} \tag{2}$$

$$\sigma_t = \frac{1}{2}\sigma_c \left(m - \sqrt{m^2 + 4s} \right) \tag{3}$$

Eq. 3 can be rewritten as follows:

$$|m| = \frac{\sigma_c}{\sigma_t}\left\{ s - (\frac{\sigma_t}{\sigma_c})^2 \right\} \tag{4}$$

Hoek and Brown's empirical failure criterion considers two types of failure [6]:

(i) Tensile failure:

This occurs when:

$$\sigma_3 < \sigma_t = \frac{1}{2}\sigma_c \left(m - \sqrt{m^2 + 4s} \right).$$

The strength/stress ratio is calculated as:

$$\frac{\sigma_t}{\sigma_3} = \frac{\sigma_c \left(m - \sqrt{m^2 + 4s} \right)}{2\sigma_3},$$

where σ_t is the uniaxial tensile strength of the rock sample.

(ii) Shear failure:

The strength/stress ratio for this condition is given by:

$$\frac{\sigma_3 + \sqrt{m\sigma_c\sigma_3 + s\sigma_c^2}}{\sigma_1}.$$

Little information was available on the m and s values for the Niobec mine rocks. However, the *RQD's* for the limestone, the intact and altered carbonatite are estimated as 90%, 95% and 90%, respectively. They are all representative of very good quality rock mass. As discussed in Section 3.2.1, it is not unreasonable to assume that the altered carbonatite has a compressive strength of 45 MPa. Thus, the tensile strength can be assumed to be one tenth of its compressive strength, i.e., 4.5 MPa. Based on these

values and using Eq.2 and Eq.4, m and s were estimated as 4.95 and 0.25 respectively. The same values were assumed for the intact carbonatite, and the limestone.

Analytic studies were carried out using m = 4.95 and s = 0.25 for the altered and intact carbonatite, and limestone. The strength/stress ratio for the four sections under consideration (i.e., planes x = 102.87m, 95.25m, 88.39m and 82.29m) were calculated. No potential failure zones around the stopes were indicated.

A second series of analytic studies, using m = 3.30 and s = 0.1111 for altered carbonatite, were conducted. These lower m and s values were arrived at by assuming the compressive strength of altered carbonatite to be 30 MPa and the tensile strength 3 MPa. The strength/stress ratio maps, for the same sections as described above, are shown in Figs. 16, 17, 18 and 19. Similarly, no failure areas were observed. The smallest strength/stress ratio, 1.24, is located at the lower portion of the pillar L-102-17 (Fig. 16).

The strength/stress ratio or local factors of safety calculated for the pillars or stope walls based on the above assumptions, should be adequate against shear failure. Therefore, no imminent shear failure is anticipated. However, Hoek & Brown's empirical failure criterion does not consider the orientation of joints. Therefore, in a tensile zone, even when the strength/stress ratio is greater than one, tensile failure is still possible depending on joint orientation.

3.3 Average Pillar Stresses and Strength

The average pillar stresses for L-102-17 and T-102-19 were evaluated based on the vertical stresses acting at the middle height of each pillar. The average vertical pillar stresses for L-102-17 and T-102-19 are 4.97 MPa and 4.12 MPa , respectively. Average pillar stresses in the transverse direction were also evaluated for L-102-17 and T-102-19; they are 13.98 MPa and 11.27 MPa, respectively. These pillar stresses appear to be low as compared to the estimated in-situ strength of the pillar.

It is a recognized fact that there is a strength reduction with increasing specimen or block size for most rocks. An approximate relationship between uniaxial compressive strength and specimen size for a number of rock types has been developed by Hoek and Brown [5]:

$$\sigma_c = \sigma_{c50} \left(\frac{50}{d}\right)^{0.18}$$

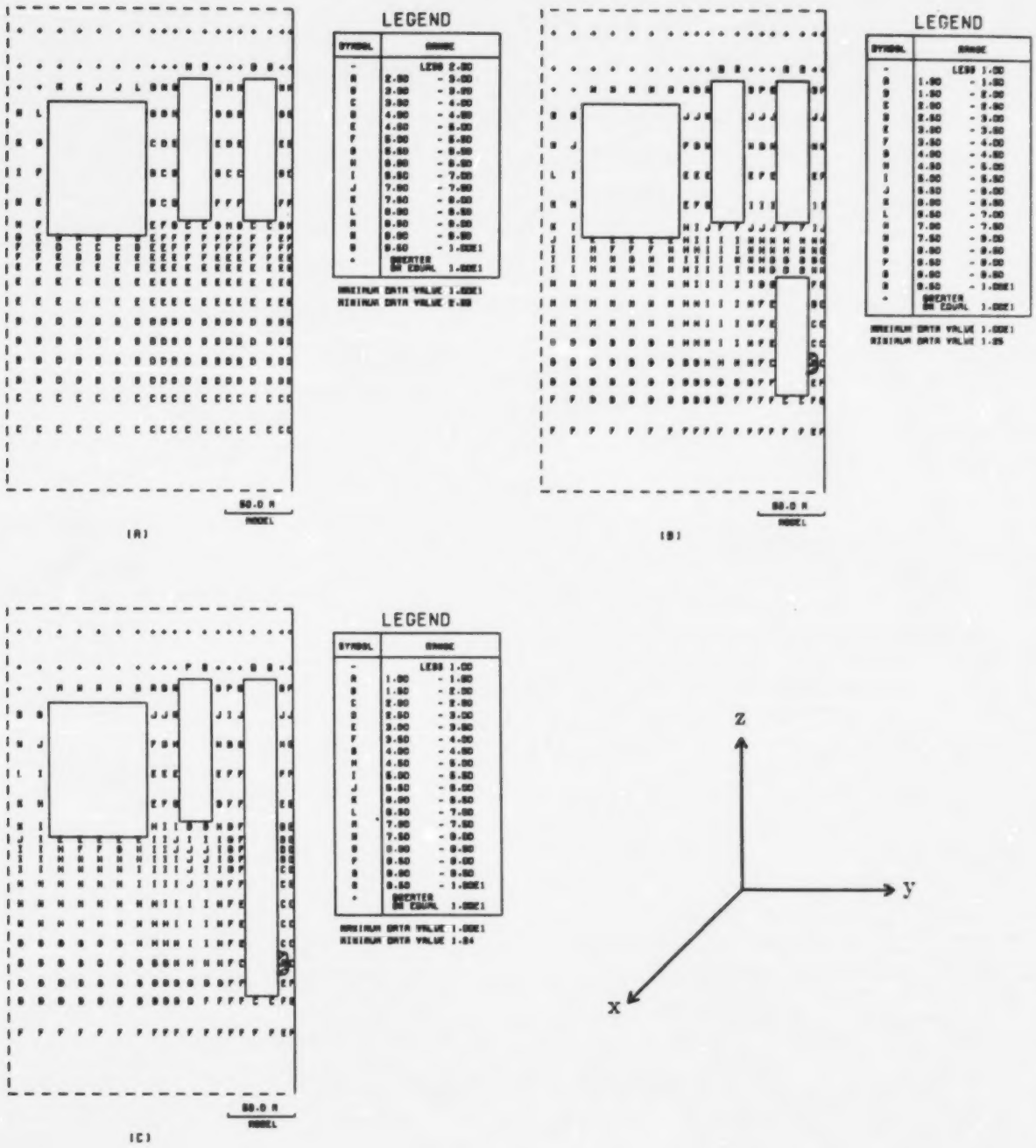

Fig. 16 Strength/stress ratio - Hoek & Brown's empirical failure criterion ($m = 3.30$, $s = 0.1111$) for section x = 102.87m: (A) mining stage 1, (B) mining stage 2, and (C) mining stage 3.

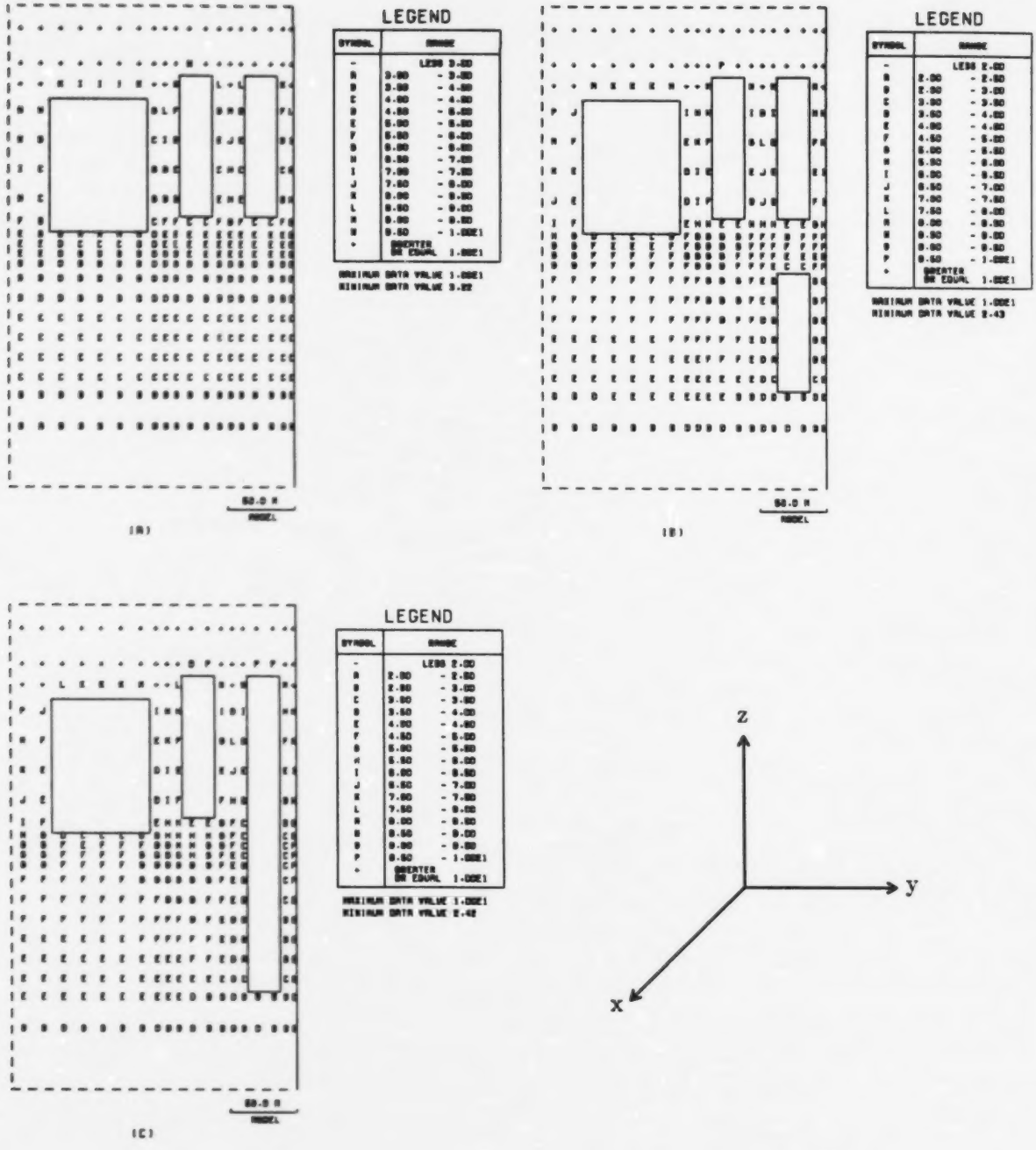

Fig. 17 Strength/stress ratio - Hoek & Brown's empirical failure criterion ($m = 3.30$, $s = 0.1111$) for section x = 95.25m: (A) mining stage 1, (B) mining stage 2, and (C) mining stage 3.

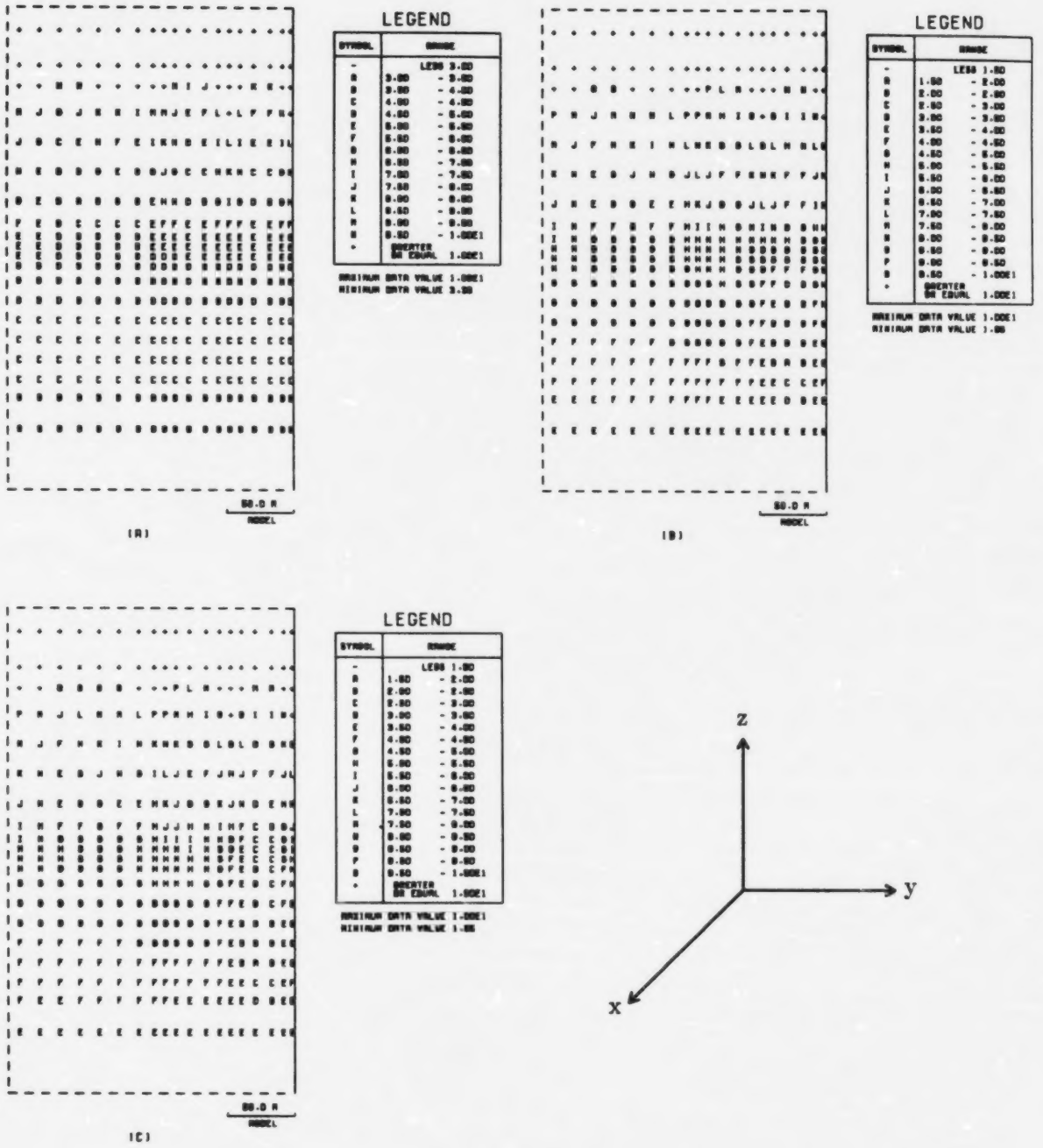

Fig. 18 Strength/stress ratio - Hoek & Brown's empirical failure criterion ($m = 3.30$, $s = 0.1111$) for section x = 88.39m: (A) mining stage 1, (B) mining stage 2, and (C) mining stage 3.

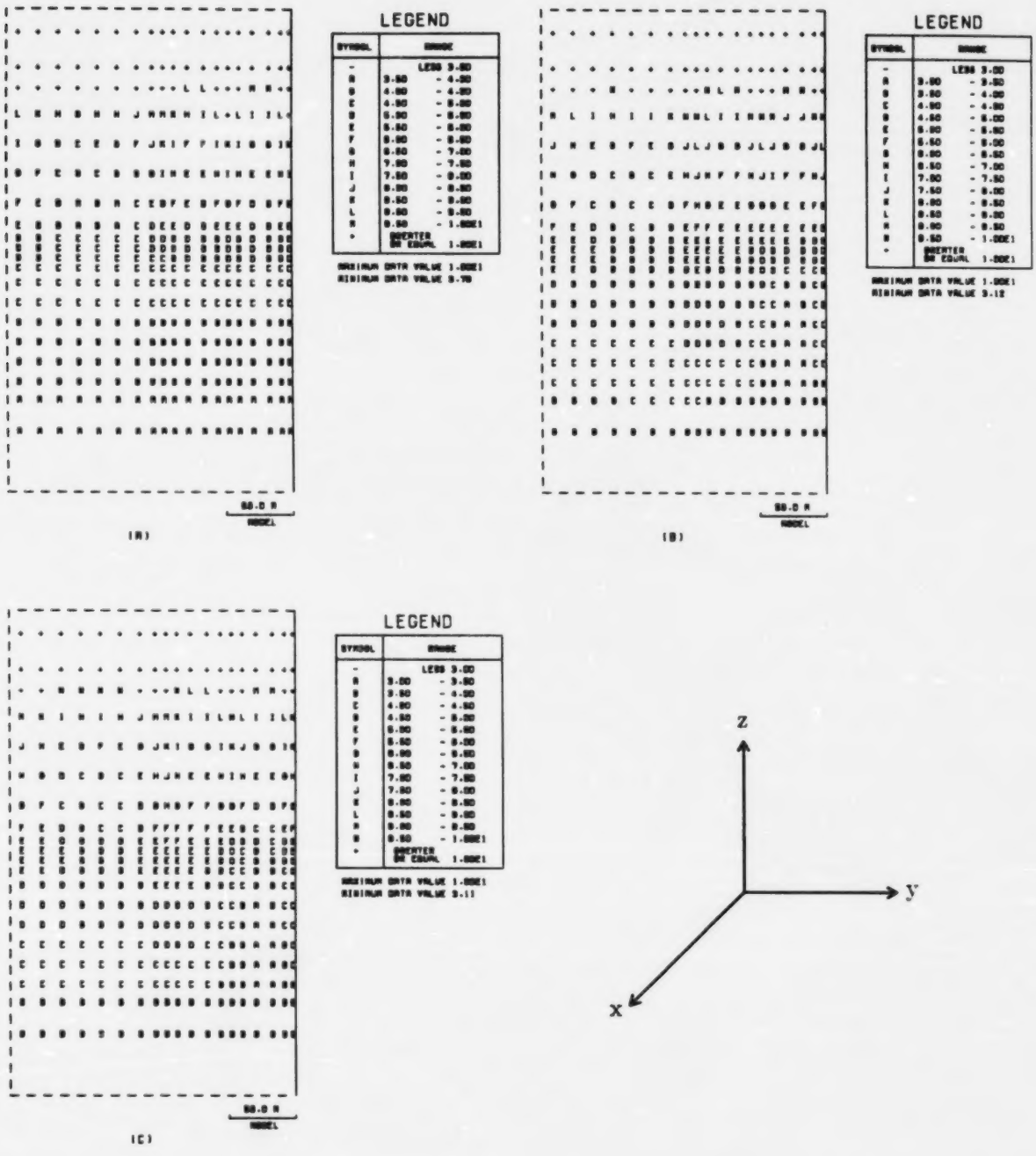

Fig. 19 Strength/stress ratio - Hoek & Brown's empirical failure criterion ($m = 3.30$, $s = 0.1111$) for section x = 82.29m: (A) mining stage 1, (B) mining stage 2, and (C) mining stage 3.

where

σ_{c50} = *the uniaxial compressive strength of a specimen of 50mm diameter*;

d = *the diameter of the specimen in mm.*

Although this relationship is derived from laboratory tests on unjointed intact rock, it may be used as a crude indication of pillar strength.

Pillar L-102-17 has a dimension of 24.39m by 24.39m in plan. The equivalent diameter of a cylindrical pillar would be approximately 13.76m (13,760mm). Thus, the pillar strength, ignoring the effect of height, is estimated as:

$$90.0 \times (\frac{50.0}{13,760.})^{0.18} = 90.0 \times 0.3638 = 32.74\ MPa$$

This seems to be a reasonable estimate. However, the actual strength of the pillar would be higher because the two sides of the pillar in the E-W direction are confined.

4.0 CONCLUSIONS AND RECOMMENDATIONS

Based on this study, following are the main conclusions and recommendations:

(a) The effect of mining of C-102-17 and C-102-19 stopes (2nd level) on ground stability conditions around C-102-23 stope and its adjacent areas, will be nominal.

(b) As expected, the mining of C-102-17 and C-102-19 stopes will induce higher compressive stresses in the lower portion of the stopes. Compressive stress levels of about 22 MPa are developed near the stope floor; however, they are not sufficiently high to cause a ground stability problem.

(c) This study also indicates that after the partial removal of the sill pillar (S-L-102-17, stage 3 mining), the height of L-102-17 pillar will exceed 235m. Localized tensile failure may occur at about one-eighth of the pillar height measured from the pillar toe. If failure develops, it may jeopardize the integrity of L-102-17 pillar and possibly the stability of stopes in the upper level (300 level) as well. Therefore, it is not recommended to remove the sill pillar at an early stage. In view of this situation, more model studies are required to arrive at a most favorable mining sequence.

(d) Based on the Drucker/Prager yield criterion, as well as Hoek & Brown's empirical failure criterion, a series of stability analysis studies was carried out. The values of

4 MPa, 40°, 3.30, and 0.1111, for cohesive strength C, angle of internal friction ϕ, and empirical constants m and s, respectively, were used in the analyses. Results indicated no potential failure zones as developing around the stopes. The material properties assumed in both analyses were considered conservative. Therefore, shear failure is not anticipated. If failure should occur, it would be localized tension failure rather than shear failure.

(e) Tensile stresses occur in stope walls, and pillars. Although these stresses are small (0 - 1.9 MPa) when compared with the tensile strength of carbonatite (5 -10 MPa), localized tensile failure may develop if joints are oriented unfavorably with respect to tensile stresses. In other words, the structural stability of the pillars will be greatly influenced by the presence of vertical or sub-vertical joints. The area for potential tensile failure is located at the lower portion of L-102-17 pillar.

(f) As indicated in Figs. 10, and 11, as well as in Figs 20(c) and 20(d) of Appendix A, tensile stresses may penetrate approximately 9m into the N-S walls of stope C-102-23. To delineate this potential fracture zone, it would be useful if multi-wire extensometers were installed in the N-S walls of C-102-23 stope before it was fully developed. This information could be used for verification of the finite element model and increase confidence in the future use of modelling.

5.0 ACKNOWLEDGEMENTS

The excellent cooperation received from the Niobec Mine Ltd., and Centre de Recher- ches Minérales, Quebec, is acknowledged. The authors wish to thank the management of Mining Research Laboratories of CANMET for their encouragement and support in this project. The authors also wish to thank G.E. Larocque, Manager of Canadian Mine Technology Laboratory, for editing the report.

6.0 REFERENCES

1. Yu, Y.S., S. Vongpaisal, Toews, N.A. and Wong, A.S.; "A Preliminary Stability Assessment of C-102-23 Stope of the Niobec Mine Under Gravitational Loading"; Division Report M&ET/MRL 86-97 (TR); Mining Research Laboratories, CANMET, Energy, Mines and Resources Canada; July, 1986.

2. Yu, Y.S., S. Vongpaisal, Toews, N.A. and Wong, A.S.; "Stability Assessment of C-102-23 Stope of the Niobec Mine Under Tectonic Stresses - Part II"; Division

Report M&ET/MRL 86-145 (TR); Mining Research Laboratories, CANMET, Energy, Mines and Resources Canada; Dec., 1986.

3. Arjang, B.; "Field Stress Determinations at the Niobec Mine, Chicoutimi, Quebec"; Division Report MRL 87-15 (TR); Mining Research Laboratories, CANMET, Energy, Mines and Resources Canada; Dec., 1986.

4. Labrie, D.; "Étude de Stabilité á la Mine Niobec"; Project STM-526, Centre de Recherches Minérales, Quebec; October, 1986.

5. Hoek, E., and Brown, E.T.; "Underground Excavations in Rock"; Stephen Austin and Sons Ltd., Hertfort, England; 1980.

6. Elsayed Armed Eissa; "Stress Analysis of Underground Excavations in Isotropic and Stratified Rock Using the Boundary Element Method"; Ph.D Thesis, Imperial College of Science and Technology, 1980.

7. Bétournay, M.C., Gorski, B. and Situm, M.; "Tétrauville Limestone of the Niobec Surface Crown Pillars: Comparison of Strength and Deformation Properties from Various Tests"; Division Report M&ET/MRL 86-144 (TR); Mining Research Laboratories, CANMET, Energy, Mines and Resources Canada; Dec., 1986.

Appendix A - Stress Components (σ_x, σ_y and σ_z) Contour Maps

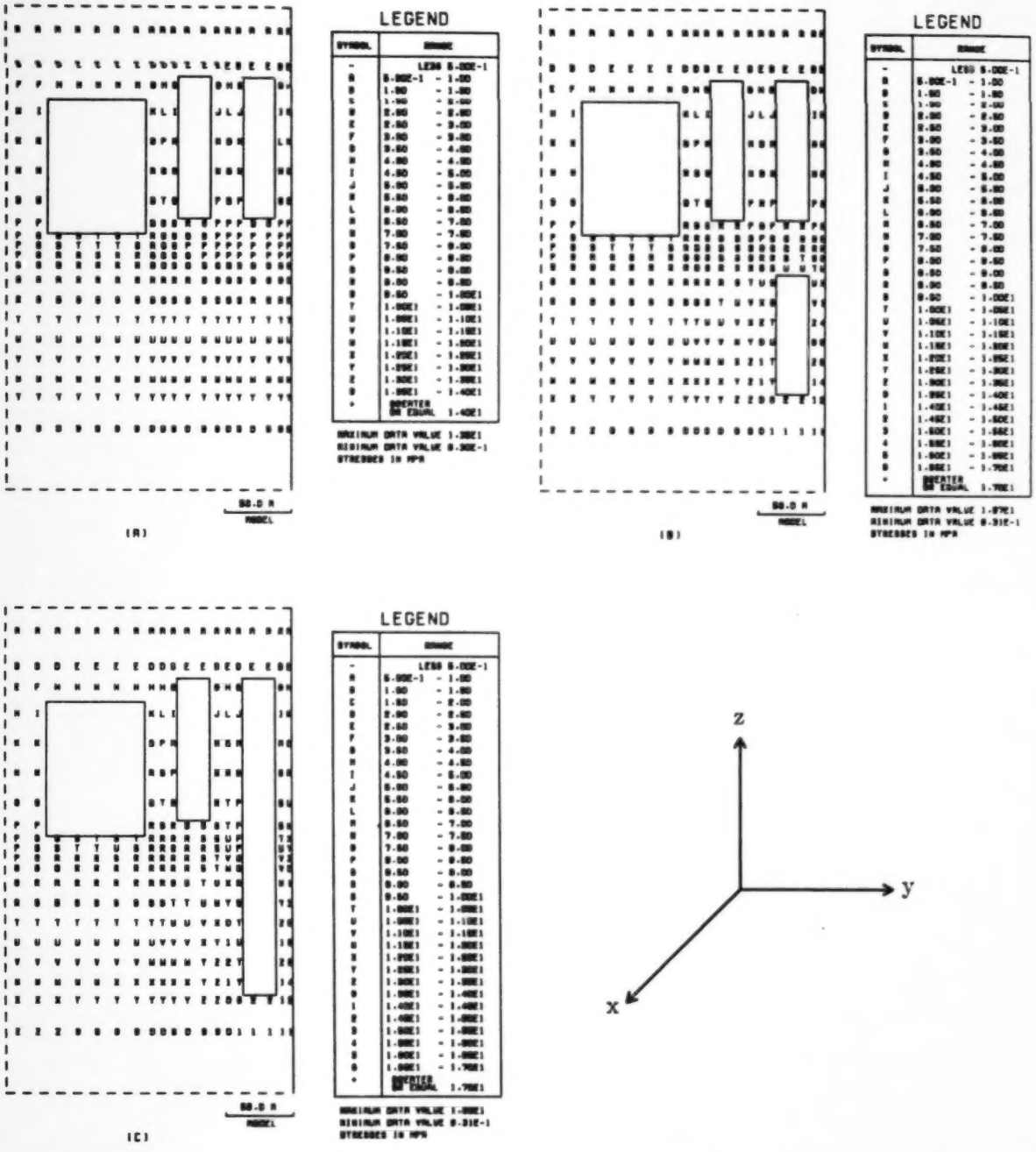

Fig. 20(a) σ_z stress contour plot for section x = 102.87m:
(A) mining stage 1, (B) mining stage 2, and (C) mining stage 3.

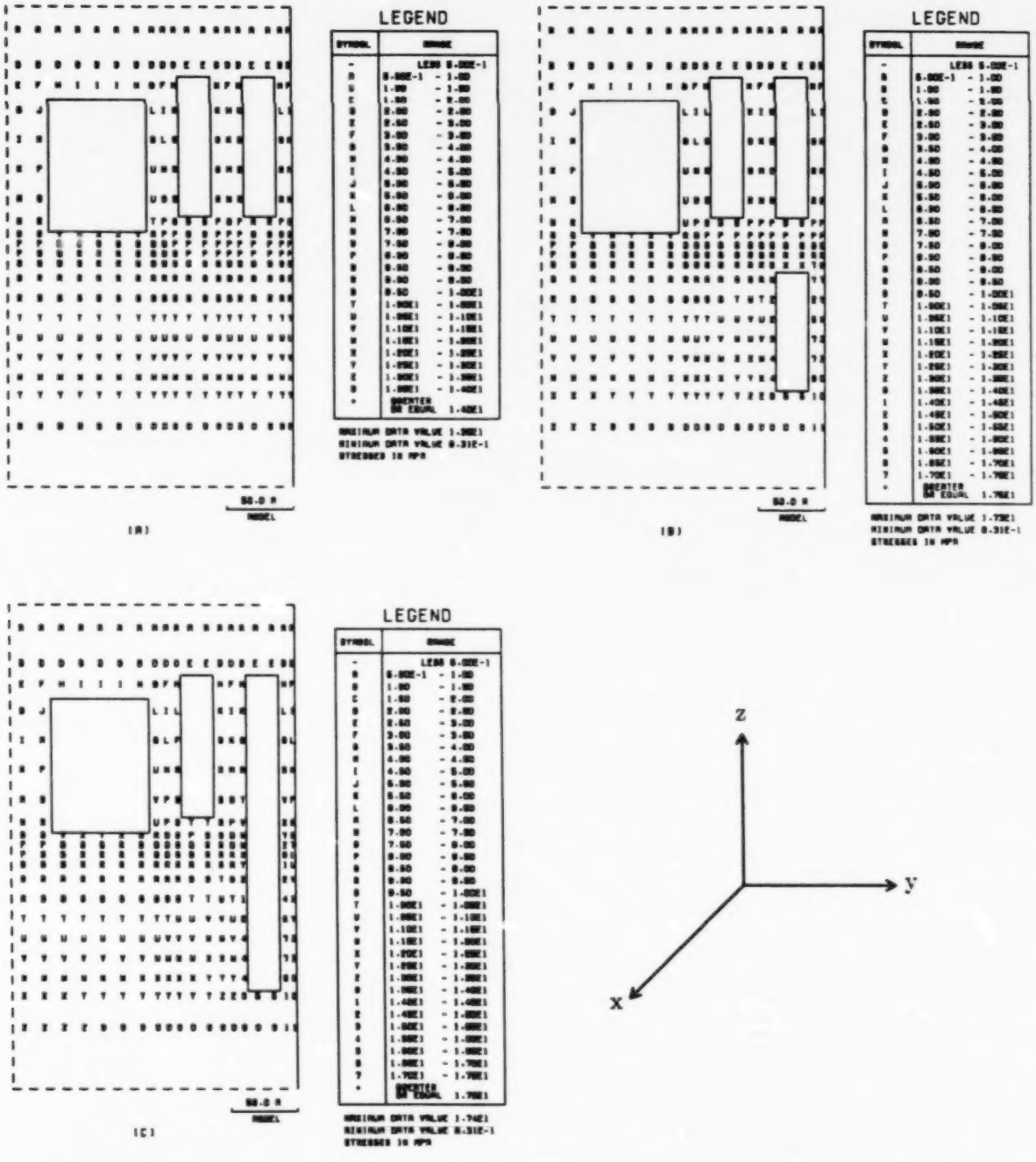

Fig. 20(b) σ_x stress contour plot for section x = 95.25m:
(A) mining stage 1, (B) mining stage 2, and (C) mining stage 3.

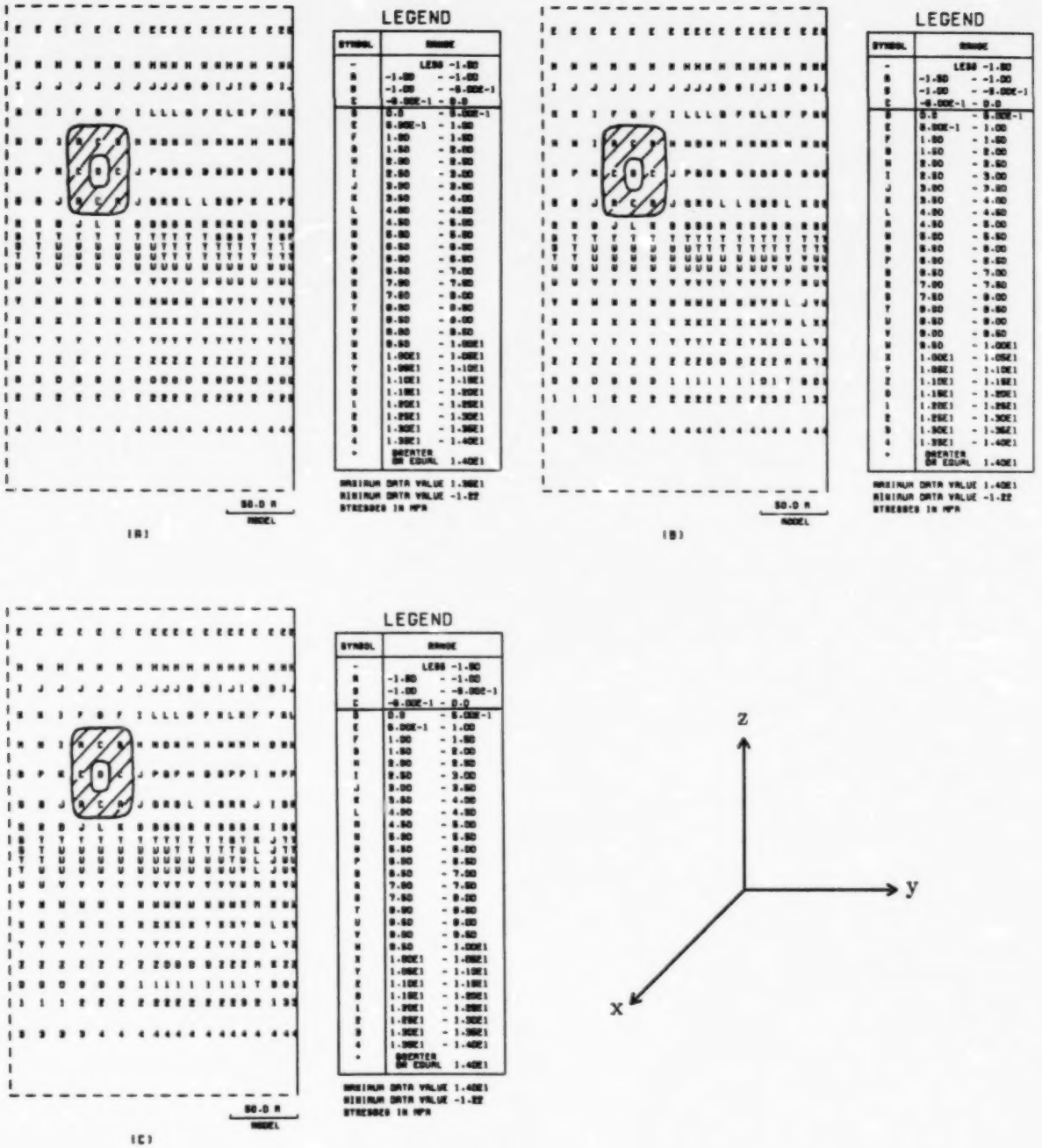

Fig. 20(c) σ_z stress contour plot for section x = 88.39m:
(A) mining stage 1, (B) mining stage 2, and (C) mining stage 3.

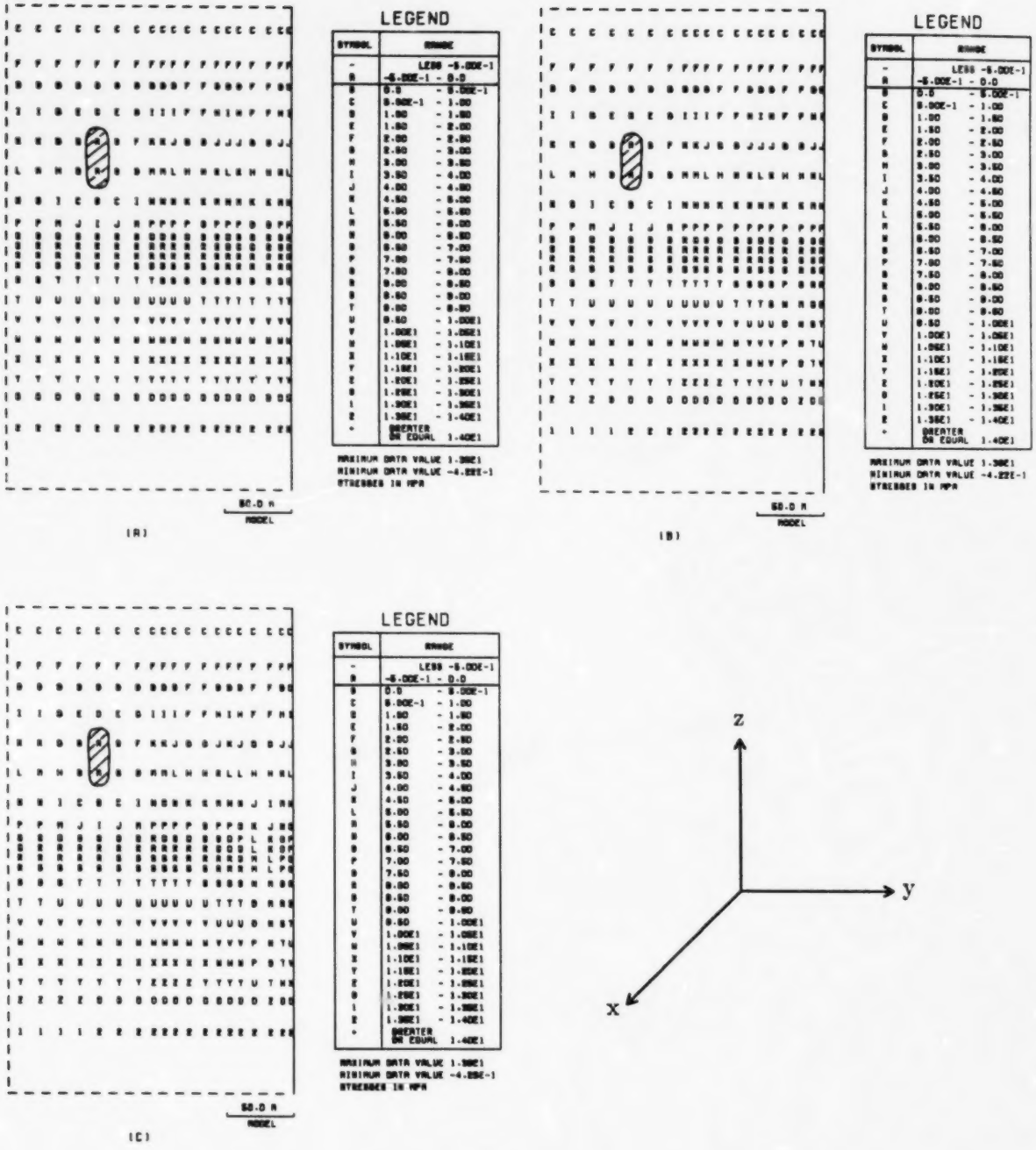

Fig. 20(d) σ_x stress contour plot for section x = 82.29m:
(A) mining stage 1, (B) mining stage 2, and (C) mining stage 3.

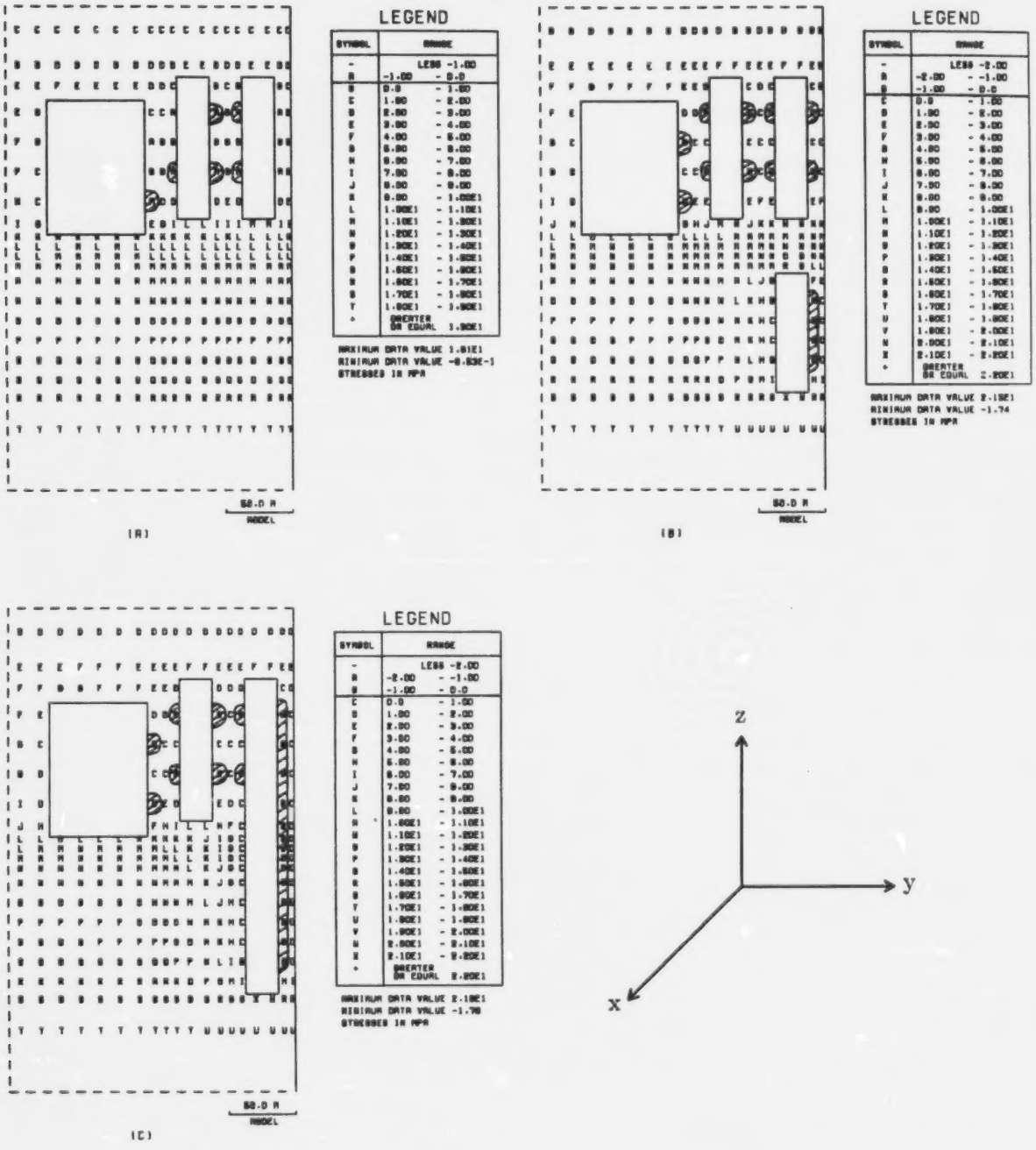

Fig. 21(a) σ_y stress contour plot for section x = 102.87m:
(A) mining stage 1, (B) mining stage 2, and (C) mining stage 3.

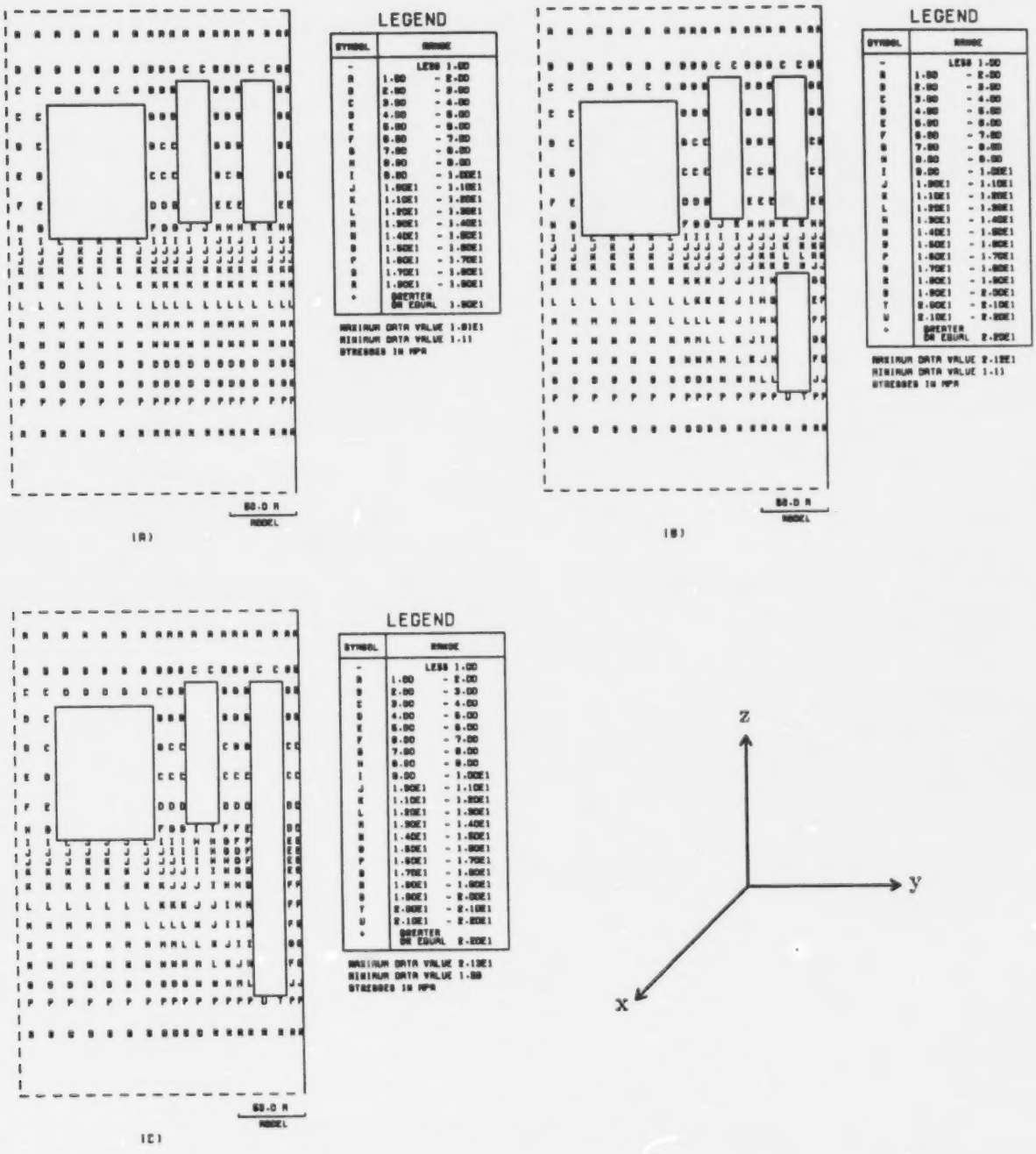

Fig. 21(b) σ_y stress contour plot for section x = 95.25m:
(A) mining stage 1, (B) mining stage 2, and (C) mining stage 3.

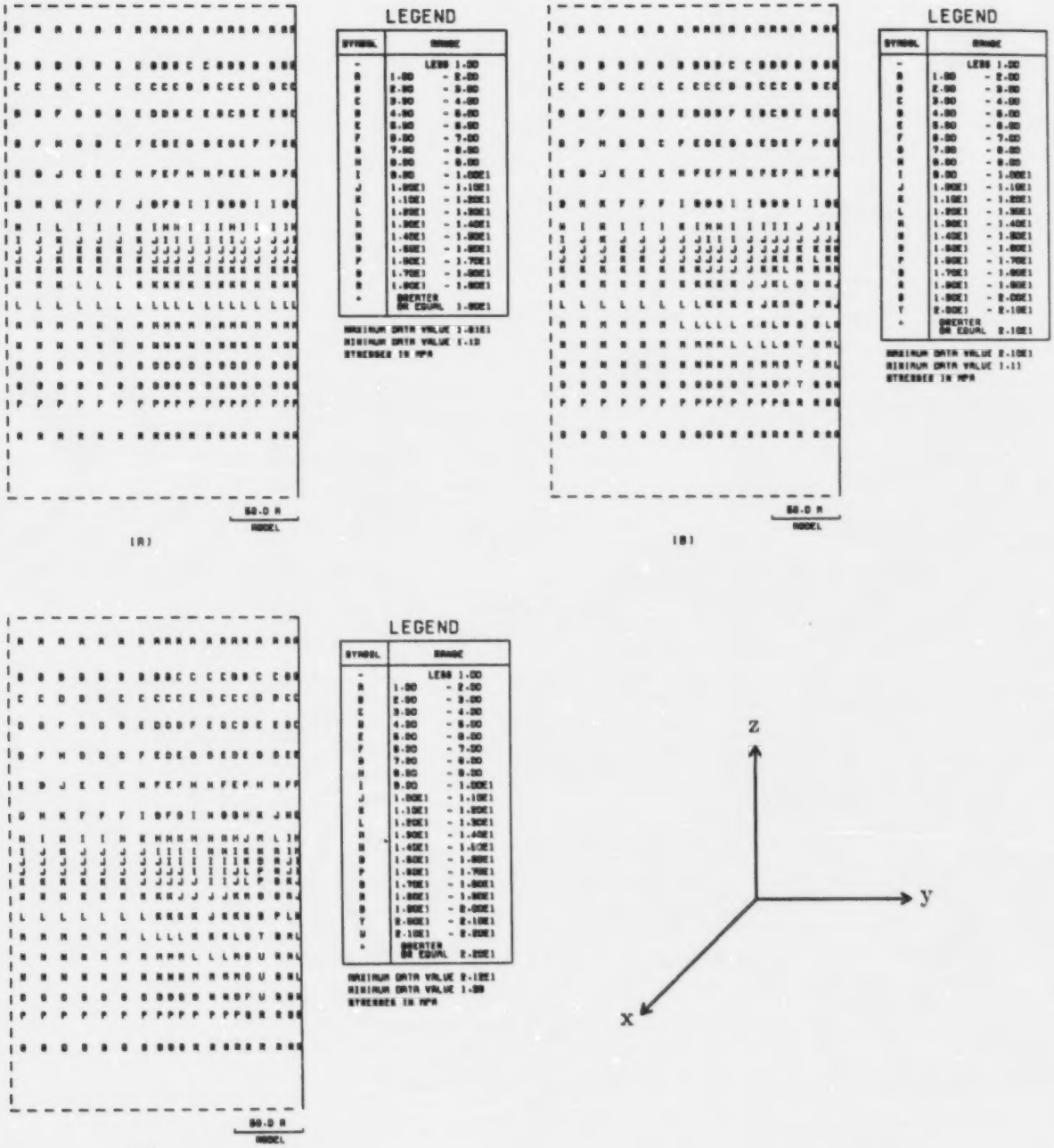

Fig. 21(c) σ_y stress contour plot for section x = 88.39m:
(A) mining stage 1, (B) mining stage 2, and (C) mining stage 3.

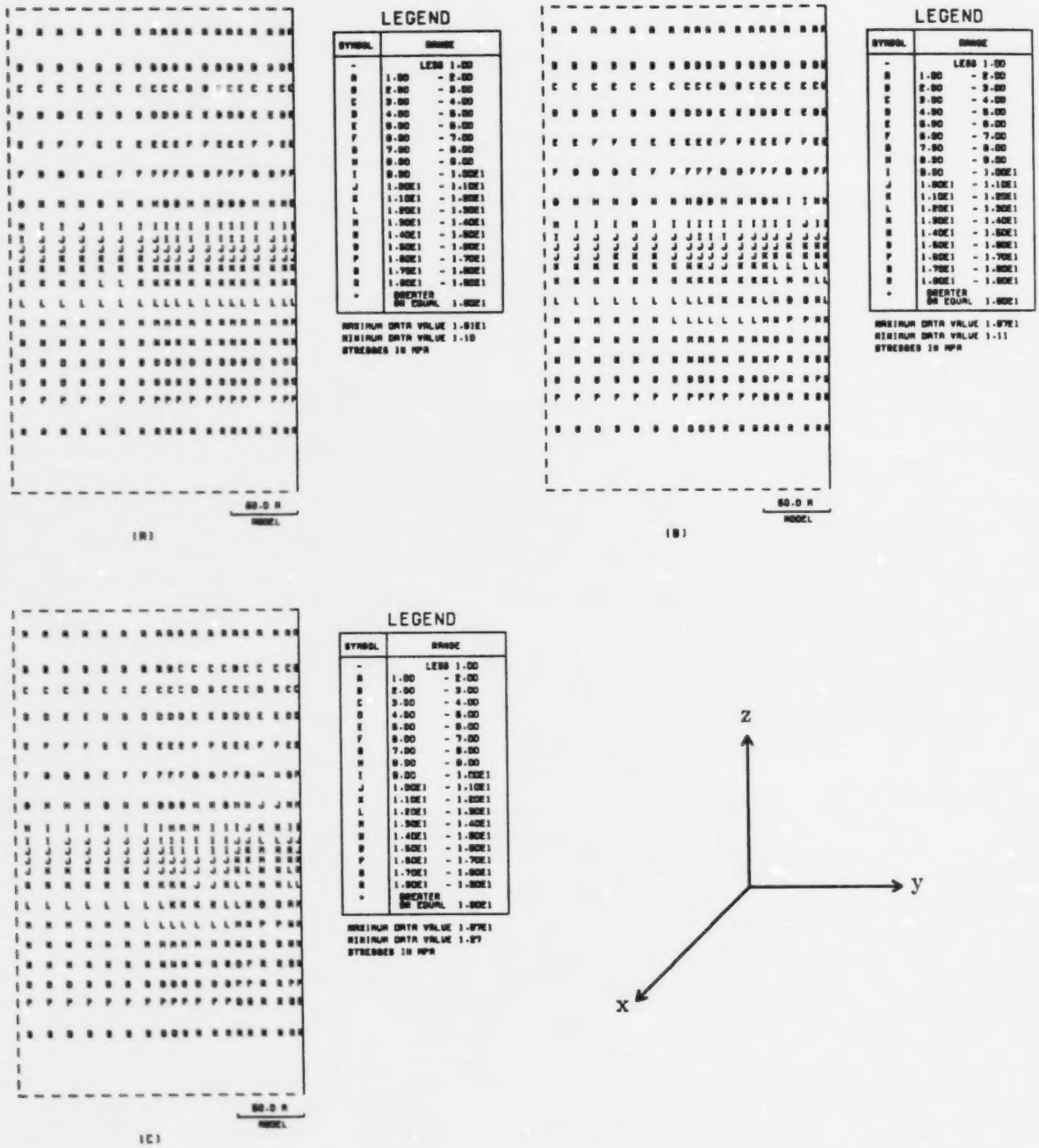

Fig. 21(d) σ_y stress contour plot for section x = 82.29m:
(A) mining stage 1, (B) mining stage 2, and (C) mining stage 3.

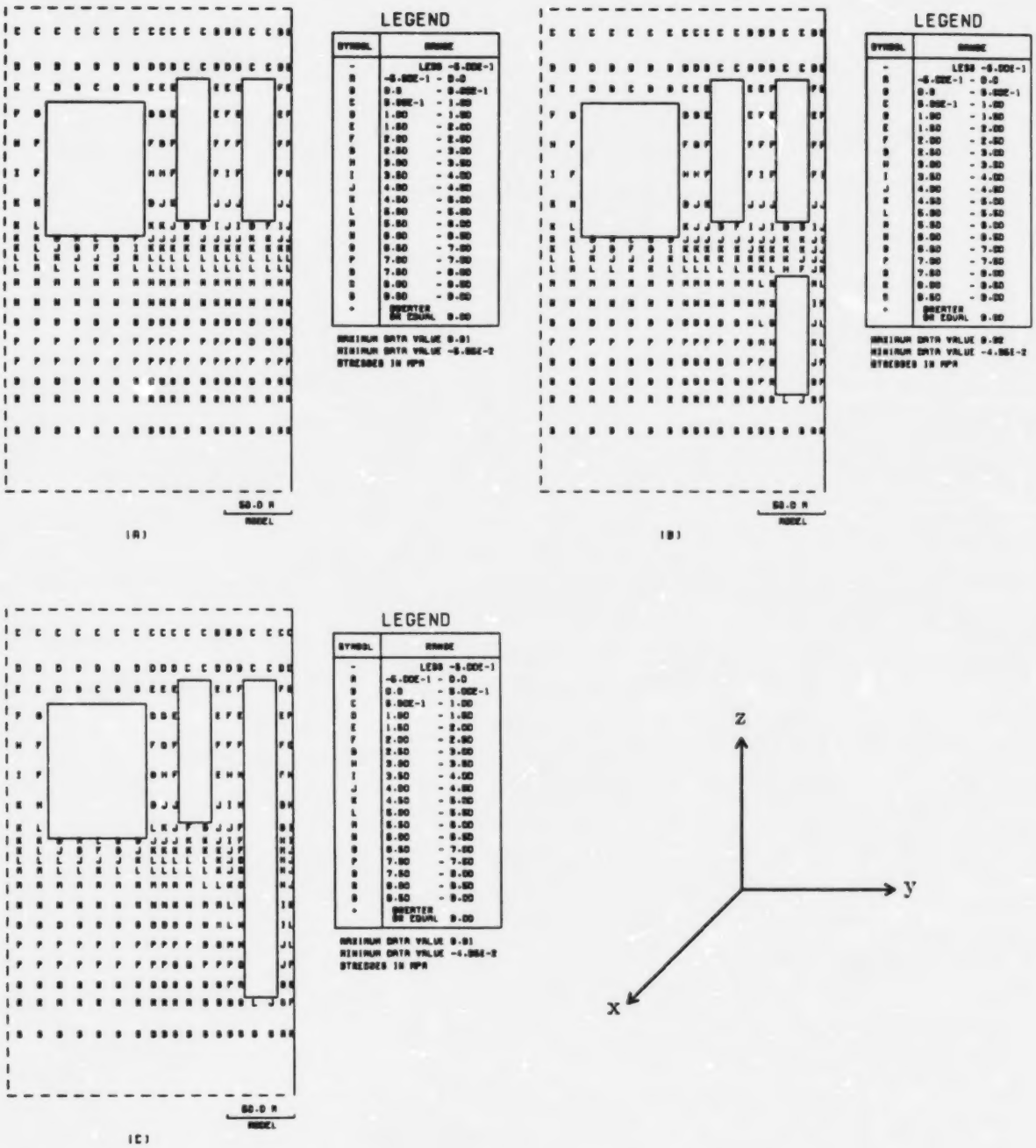

Fig. 22(a) σ_z stress contour plot for section x = 102.87m:
(A) mining stage 1, (B) mining stage 2, and (C) mining stage 3.

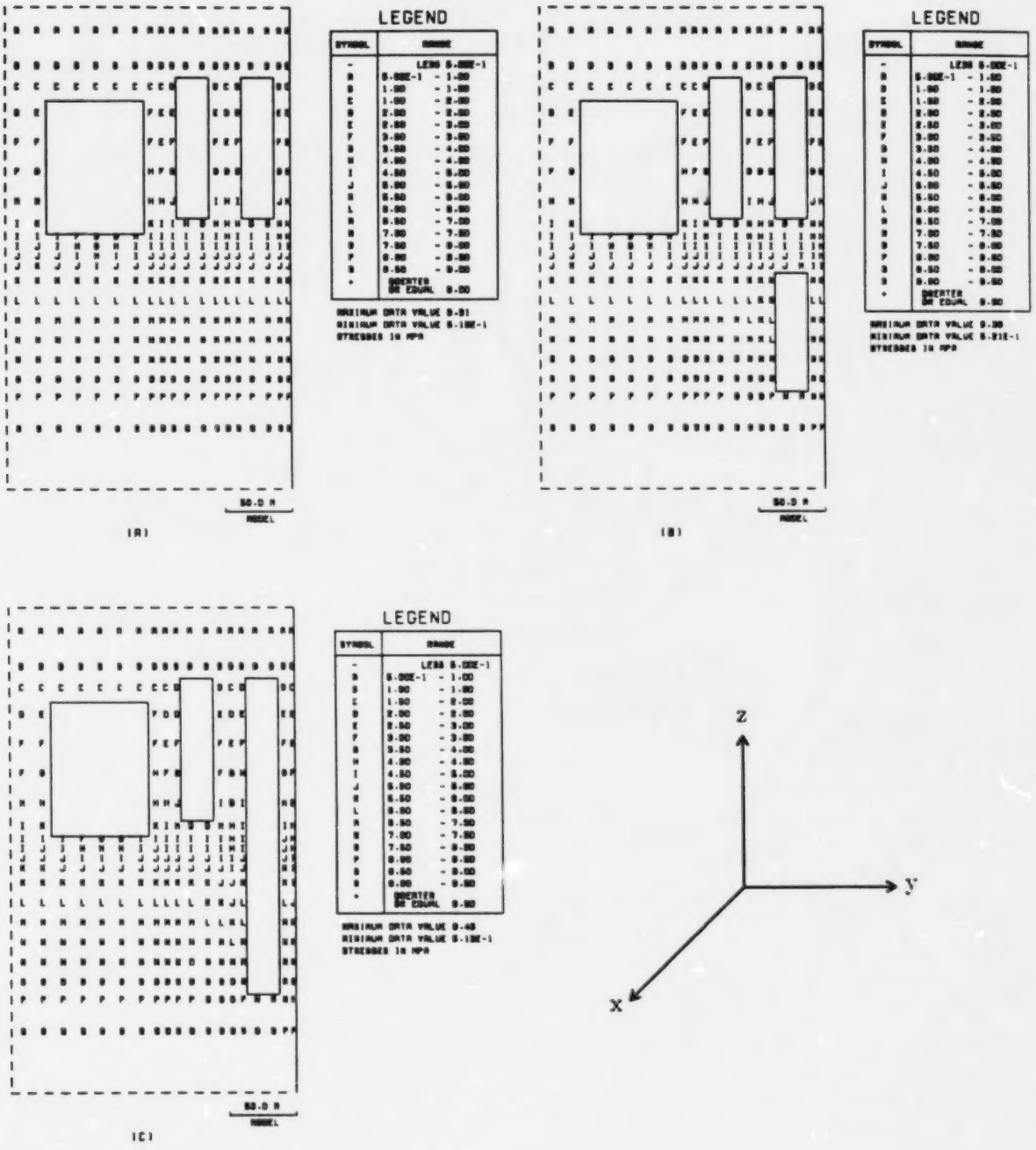

Fig. 22(b) σ_z stress contour plot for section x = 95.25m:
(A) mining stage 1, (B) mining stage 2, and (C) mining stage 3.

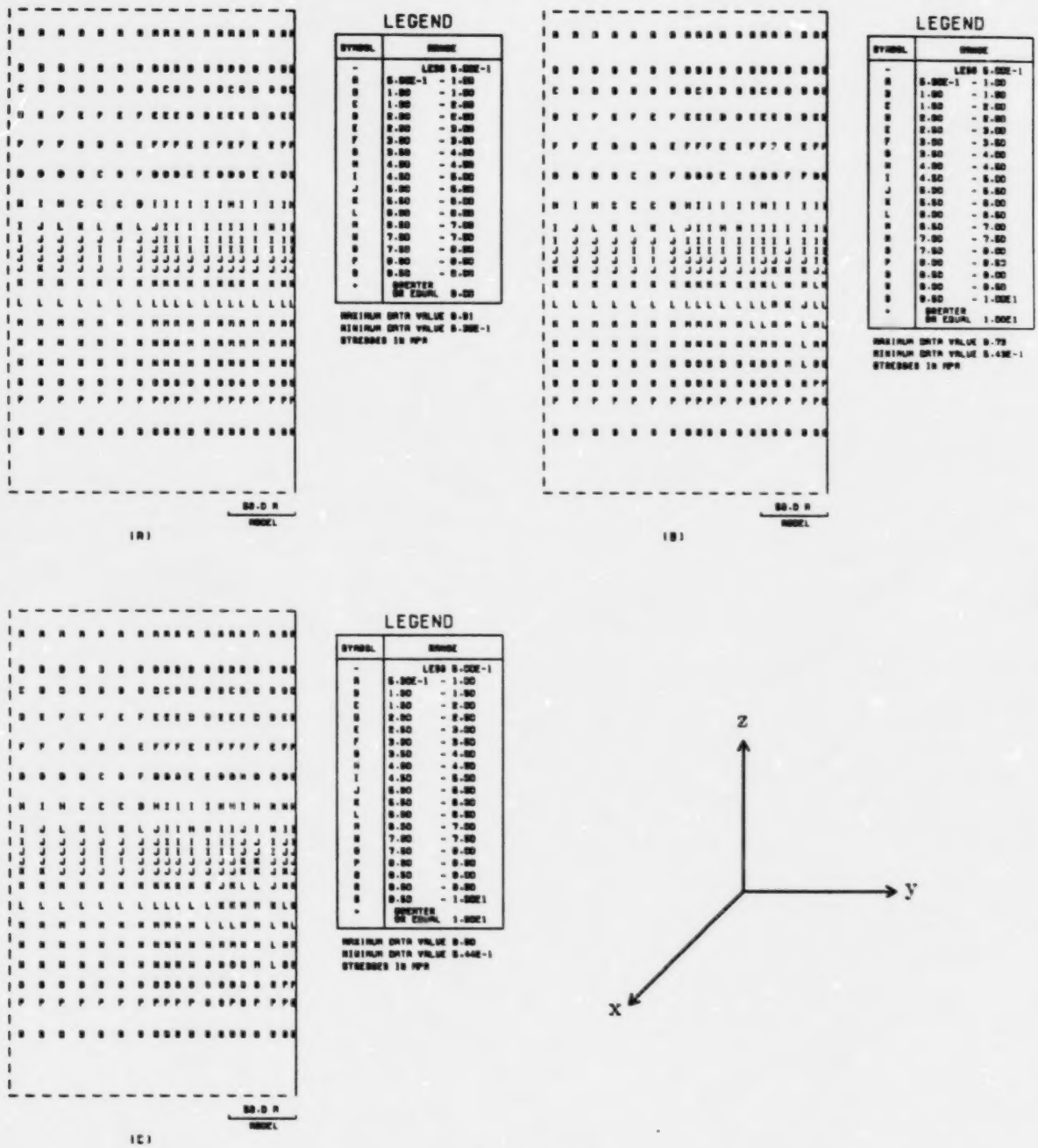

Fig. 22(c) σ_z stress contour plot for section x = 88.39m:
(A) mining stage 1, (B) mining stage 2, and (C) mining stage 3.

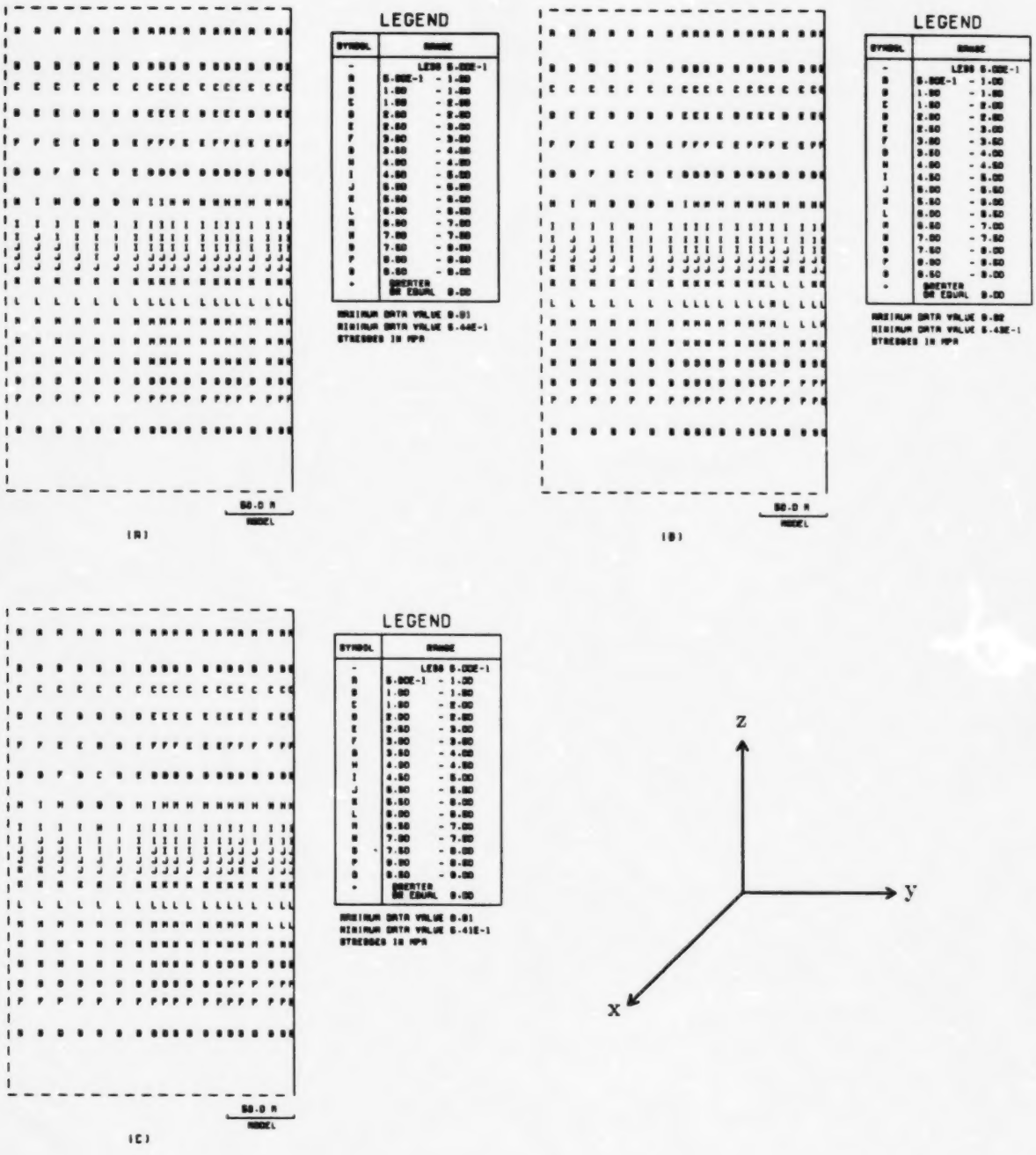

Fig. 22(d) σ_z stress contour plot for section x = 82.29m:
(A) mining stage 1, (B) mining stage 2, and (C) mining stage 3.